Synthesis and Reduction of Iron(III) Porphinone Complexes and Their Spectroscopy Studies

Yanyan Huang
Marquette University

SYNTHESIS AND REDUCTION OF IRON(III) PORPHINONE COMPLEXES AND THEIR SPECTROSCOPY STUDIES

by

Yanyan Huang, B. S.

A Thesis submitted to the Faculty of the Graduate School,
Marquette University,
in Partial Fulfillment of the Requirements for
the Degree of the Master of Science

Milwaukee, Wisconsin

December 2010

ABSTRACT
SYNTHESIS AND REDUCTION OF IRON(III) PORPHINONE COMPLEXES AND THEIR SPECTROSCOPY STUDIES

Yanyan Huang, B.S.

Marquette University, 2010

The vibrational spectra of iron(I) porphinone, and related species were studied in this work. The iron(I) complexes were synthesized by the sodium anthracenide reduction method. The extent of reduction was monitored by UV-visible spectroscopy. The products were precipitated with heptane. Efforts to obtain single crystals of the iron(I) complex were unsuccessful, but procedures for further work were developed. The deuteration of the methylene protons was studied. These macrocycles of these complexes can be used for further studies by vibrational spectroscopy. The infrared and resonance Raman spectra of iron(I) porphinone in KBr were obtained and interpreted. Further studies using deuterated macrocycles and DFT calculations can be used to better understand the electronic structures of the formal iron(I) state.

ACKNOWLEDGMENTS

Yanyan Huang, B.S.

First of all, I wish to express my appreciation and thanks to my research advisor, Dr. Michael D. Ryan for his guidance, encouragement and patience throughout my stay at Marquette University. I also want to extend my sincere gratitude to my thesis committee members, Dr. Adam Fiedler and Dr. Mark G. Steinmetz for their time in reading my dissertation and kindly suggestion.

I would also like to express my appreciation to Dr. James R. Kincaid and Dr. Piotr J. Mak for the help and guidance of the resonance Raman Spectroscopy. Finally, I would want to dedicate this work to my husband, Yibin and my family for the invaluable support, love and patience. Without them, I can't achieve the goal today.

CONTENT

LIST OF TABLES

LIST OF FIGURES

CHAPTER ONE

INTRODUCTION

1-1. Porphyrins and their deuteration

Porphyrins are heterocyclic macrocycles which consist of four pyrrole subunits interconnected at their α-carbon atoms via methine bridges (=CH-). Porphyrins are aromatic, and obey Hückel's rule for aromaticity in that they possess 4n+2 π (26π electrons in total) electrons that are delocalized over the macrocycle[1]. The saturation of one pyrrole double bond results in a chlorin. The reduction of the double bonds forms bacteriochlorins and isobacteriochlorins. The structures of the porphyrins and their derivatives are shown in Figure 1-1.

Deuterium exchange reactions of porphyrins provide a method of studying the electronic structure of the porphyrin macrocycle. Deuterium substituted compounds have found wide spread application in physical chemical studies including vibration, NMR and EPR spectroscopy. The low-yield multistep syntheses of the free base porphyrins often make a simple exchange process on preformed porphyrins the best route to these materials. Label incorporation can be accomplished either by total synthesis or by an exchange of one or more sites on the assembled porphyrins. Deuterium labeling of porphyrins has been largely studied in two positions: exchange at the meso positions and exchange at the β pyrrole position. The acid catalyzed deuteration exchange reaction occurs at the meso positions[2-6].

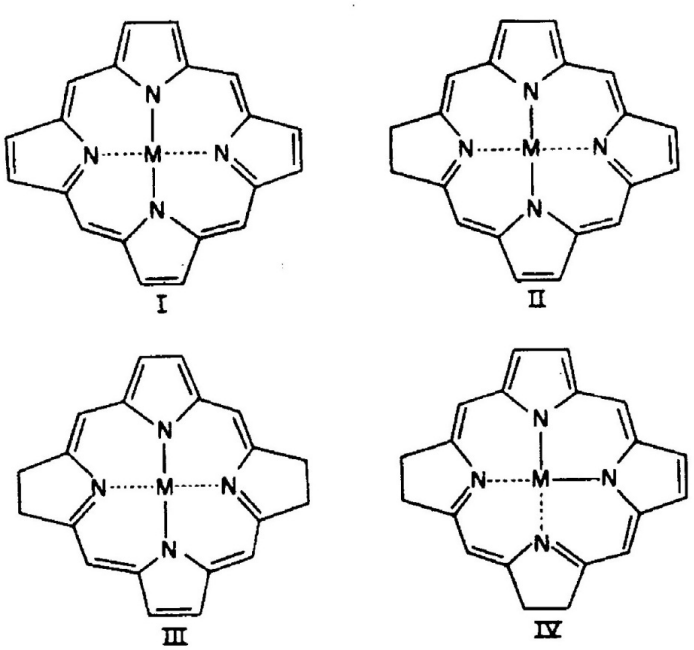

Figure 1-1. Structure formulas of metalopophryin (I), Chlorin (II), bacteriochlorin (III) and isobacteriochlorin (IV)[7]

1-2. Iron porphyrins and their derivatives

Iron porphyrins and chlorins are formed by substituting an iron atom for the two central protons of the macrocycle. Iron porphyrins or chlorins may be four, five or six coordinate with formal oxidation states for iron ranging from 0 to +4.

Generally speaking, coordination of strong field ligands results in six-coordinate, low-spin ferric and ferrous porphyrin or chlorin complexes. The typical structure of a five-coordinate ferric porphyrin complex, given in Figure 1-2, shows that the iron atom is out of the macrocyclic plane by the distance of d. For the six-coordinate iron porphyrins, the iron atoms are in, or nearly in, the plane of the macrocycle.

The energy levels and electron occupancy of the 3d orbitals of Fe^{III} (d^5), Fe^{II} (d^6) and Fe^{I} (d^7) are shown in Figure 1-3[8]. The spin state is determined by both the nature of the porphyrins and the ligands (including the axial and the substituent ligands). In general, coordination of the strong field ligands results in six-coordinate, low-spin Fe(I), Fe(II), Fe(III) complexes. Weak field ligands, such as $-Br^-$ and $-I^-$, will cause both five- and six-coordinate high-spin complexes. In certain cases, some very weak ligands, e.g. ClO_4^- and $SO_3CF_3^-$ [9, 10], give rise to five-coordinate intermediate-spin and spin-admixed intermediate ferric porphyrins. The uncomplexed ferrous porphyrins, such as Fe^{II}TPP, exist as an intermediate-spin complex.[7,11-12]

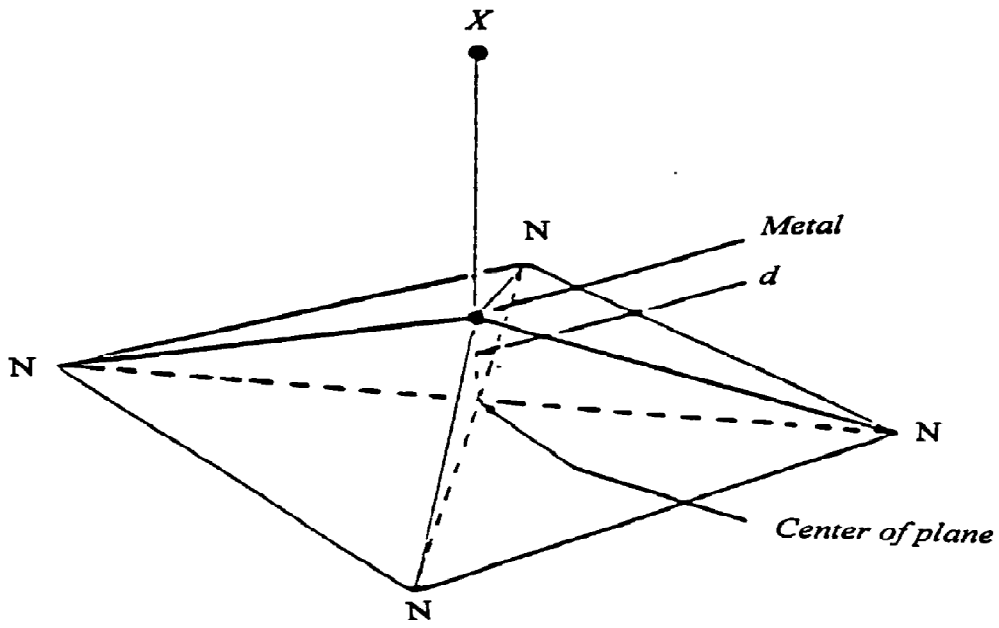

Figure 1-2. The structure of five-coordinate iron porphyrin complex

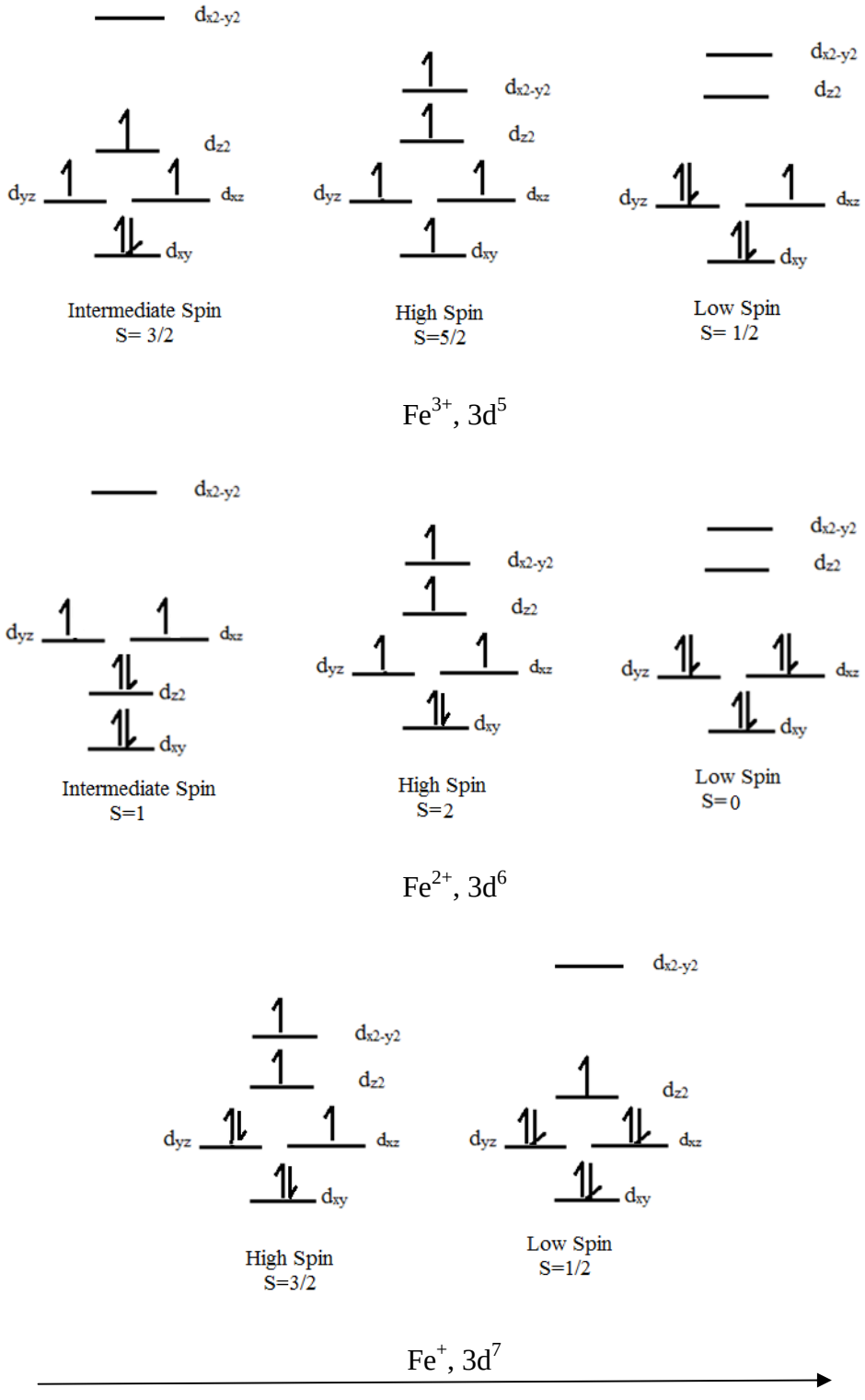

Figure 1-3. Energy levels and electron occupancy of 3d Fe(I), Fe(II) and Fe(III) porphyrin systems[8]

In the past forty years, iron porphyrins and their derivatives have been extensively studied. Generally, iron porphyrins may be reduced in three discrete sites: at the porphyrin ring, the iron or the axial ligands. For iron porphyrins, the reduction can occur at the porphyrin ring or the iron:

$$Fe^{III}(P)Cl + e^- \rightarrow Fe^{II}(P) + Cl^- \quad (1)$$

$$Fe^{II}(P) + e- \rightarrow [Fe(P)]^- \quad (2)$$

$$[Fe(P)]^- + e- \rightarrow [Fe(P)]^{2-} \quad (3)$$

Iron porphyrin complexes have been studied extensively in their common oxidation states, iron(II) and iron(III). Most properties of the iron(II) and iron(III) porphyrin complexes are understood or can be predicted with good accuracy and confidence from x-ray crystal structures, Mössbauer, proton NMR and resonance Raman spectra. The reduction of the Fe(III) to Fe(II) porphyrin complexes is quite clear now.

Two electron reduced iron porphyrins tend to be more nucleophilic as compared to the ferric and ferrous states. The ferric and ferrous states are electrophilic. The increased nucleophilicity of low valent metalloporphyrins may be important for their use as catalysts.

1-2-1. Reduction of iron tetraphenylporphyrin complexes

The structure of Fe^{III}TPPCl is shown in Figure 1-4 and is one of the most studied iron porphyrin systems. The two-electron reduction product of Fe^{III}TPPCl, designated as $[Fe(TPP)]^-$, is the so called iron(I) porphyrin complex.

The UV-visible spectra of Fe^{II}TPP and its reduction products are shown in Figure 1-5 by Reed[13]. The UV-visible spectrum of $[Fe(TPP)]^-$ in THF (wavelength/nm) are 392 (Soret), 424 (Soret), 512, 576, 605 and 674. The Q bands (wavelength/nm) of Fe^{II}TPP are 546 and 610 and the Q bands (wavelength/nm) of $[Fe(TPP)]^{2-}$ are 572 and 612.

From Reed[13], $[Fe(TPP)]^-$ was best described as a resonance hybrid between the low spin S=1/2 iron(I) porphyrin anion ($[Fe^{I}TPP]^-$) and the spin-coupled S=1 iron(II) porphyrin radical anion ($[Fe^{II}\text{-}TPP\cdot]^-$). The resonance hybrid had sufficient metal/radical orbital overlap to give an overall S=1/2 state.

$$Fe^{III}(TPP)Cl \overset{+2e}{\Longrightarrow} [Fe^{I}TPP]^- \leftrightarrow [Fe^{II}\text{-}TPP\cdot]^-$$

However, the resonance model was questioned by Bocian[14] based on the resonance Raman spectrum. The high frequency portion of the B-state-excitation (λ_{ex}=457.1 nm) resonance Raman (RR) spectrum of $[Fe(TPP)]^-$ is shown in Figure 1-6[14] (bottom).

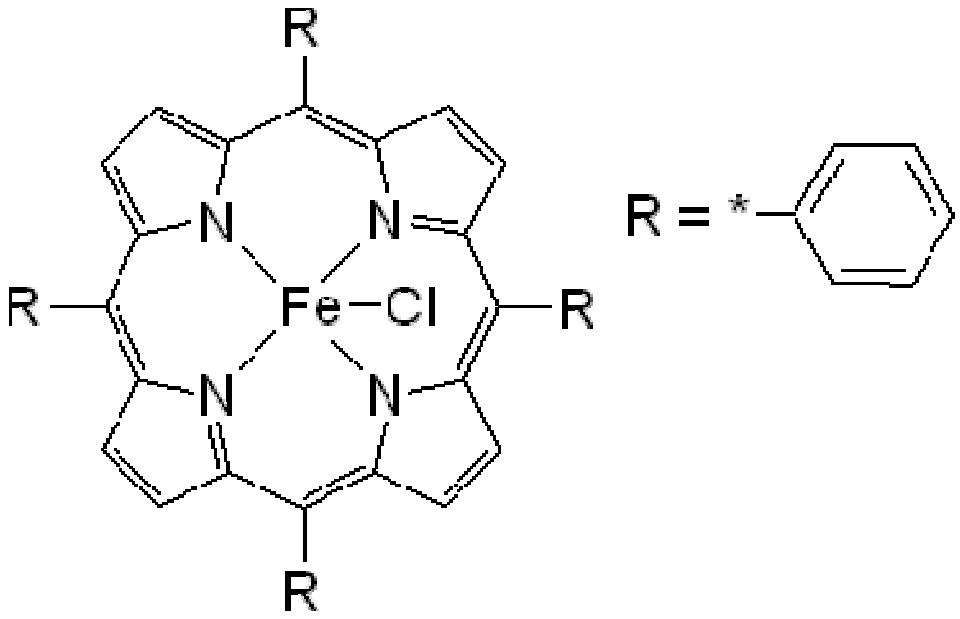

Figure 1-4. The structure of iron(III) tetraphenylporphyrin chloride

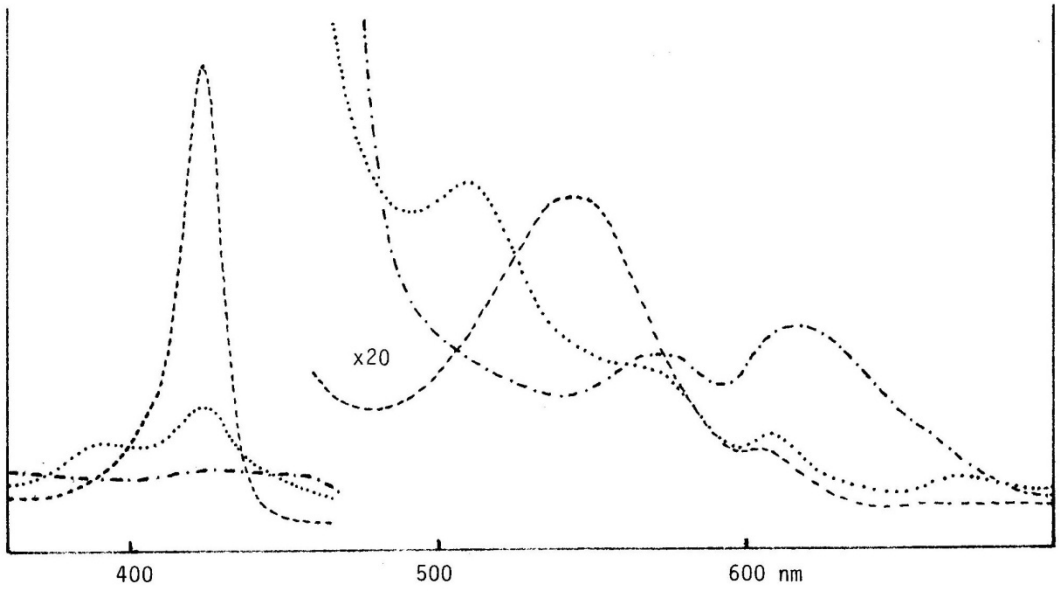

Figure 1-5. UV-Visible spectra of $Fe^{II}(TPP)$, $[Fe(TPP)]^{-}$ and $[Fe(TPP)]^{2-}$ in THF solution[13]. Key: ---, $Fe^{II}(TPP)$; ⋯, $[Fe(TPP)]^{-}$; and– · –, $[Fe(TPP)]^{2-}$.

For comparison, the RR spectra of high-spin (top) and low-spin (middle) iron(II) tetraphenylporphyrin complexes are also displayed in Figure 1-6. Bocian used the nomenclature of υ_4 and υ_2 that came from octaalkylporphyrins by Spiro[15]. The Raman frequencies (cm^{-1}) of υ_4 and υ_2 for $[Fe(TPP)]^-$, low-spin $Fe^{II}(TPP)$ and high-spin $Fe^{II}(TPP)$ are summarized in Table 1-1.

Table 1-1. The Raman frequencies of υ_4 and υ_2 modes for metal tetraphenylporphyrin complexes in DMF

	$Fe^{II}TPP$ (high-spin)	$Fe^{II}TPP$ (low-spin)	$(FeTPP)^-$	$Zn^{II}TPP$	$[ZnTPP]^-$
υ_4 (cm^{-1})	1344	***1354***	***1356***	1351	1346
υ_2 (cm^{-1})	1540	***1559***	***1555***	1548	1531

From Table 1-1, both the υ_4 and υ_2 modes of $Fe^{II}TPP$ undergo large upshifts upon conversion of the Fe^{II} ion from high to low spin. However, the υ_4 and υ_2 bands of $(FeTPP)^-$ and $Fe^{II}TPP$ (low-spin) are quite close, which are 1356 versus 1354 cm^{-1} and 1559 versus 1554 cm^{-1}. The frequencies of υ_4 and υ_2 observed for $[FeTPP]^-$ indicate a low-spin formulation for the metal center at room temperature, which is consistent with the magnetic measurements from Reed[13] and Hickman[33]. Meanwhile, the subsequent NMR measurement showed that the unpaired electron resides in the metal d_{z^2} orbital rather than the π molecular orbitals[33].

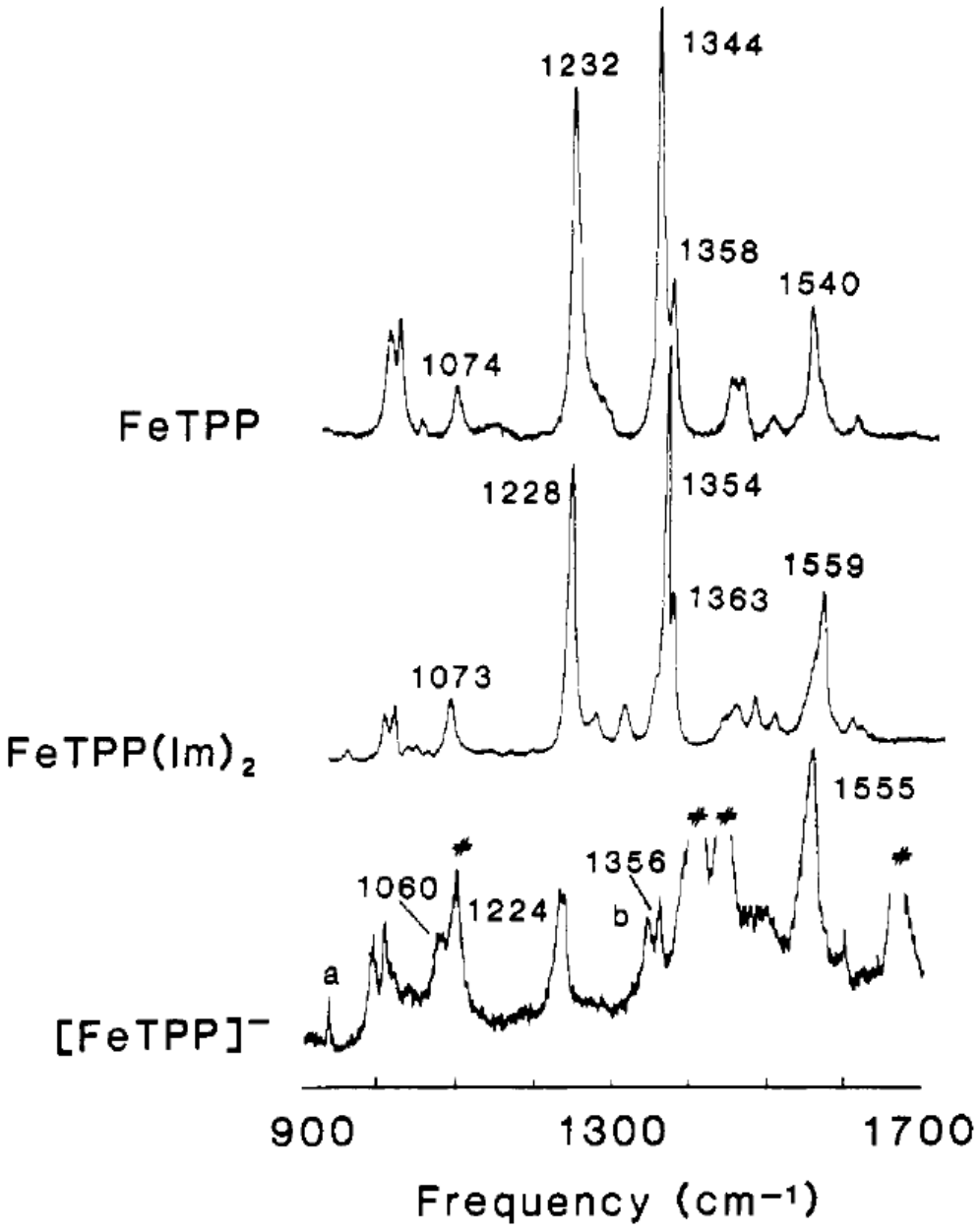

Figure 1-6. Raman Spectra of high-spin $Fe^{II}TPP$ [λ_{ex}=413.1nm (top)], low-spin $Fe^{II}TPP$ [λ_{ex}=413.1nm (middle)] and $(FeTPP)^-$ [λ_{ex}=457.9nm (bottom)] in DMF solution (N, N-dimethylformamide), 0.1M TBAP (tetrabutylammonium perchlorate). Peak a is due to TBAP. Peak b is due to $Fe^{II}TPP$. Solvent modes are denoted by #.

The resonance Raman (RR) spectra of $Zn^{II}TPP$ and $[ZnTPP]^-$ by Bocian is also included in Table 1-1. ZnTPP is known as the porphyrin macrocyclic centered reduction model: $Zn^{II}TPP \overset{+e}{\Rightarrow} [Zn^{II}(TPP\cdot)]^-$. The results are consistent with those of the former study and show that the ν_4 band is relatively insensitive to macrocycle centered reduction whereas the ν_2 band is observed to be quite sensitive to the changes in the electron density of macrocycle. The ν_2 band downshifts 17 cm^{-1} from $Zn^{II}TPP$ to $[Zn^{II}(TPP\cdot)]^-$. Since there is only 5 cm^{-1} difference of the ν_2 band from $Fe^{II}TPP$ (low-spin) to $(FeTPP)^-$, Bocian concluded that the reduction of $Fe^{II}TPP$ is a metal centered reduction. Thus, the reduced product $(FeTPP)^-$ can be described safely as an anion with a low spin iron(I) center. The reduction from the starting material $Fe^{III}TPPCl$ can be written:

$$Fe^{III}(TPP)Cl \overset{+2e}{\Longrightarrow} [Fe^{I}TPP]^- + Cl^-$$

Although the unpaired electron density resides in the d_{z^2} orbital, the 5 cm^{-1} difference of ν_2 band between low-spin $Fe^{II}TPP$ and low-spin $[Fe^{I}TPP]^-$ does allow the assessment that some of the electron density has been transferred from the metal d_π orbital to the porphyrin π orbital via back-bonding. This delocalization of additional charge onto the ring is appealing because the process provides a means of stabilizing the low valent iron ion.

If a 17 cm^{-1} shift that occurred upon reduction from $Zn^{II}TPP$ to $[Zn^{II}(TPP\cdot)]^-$ represents the effect of one addition electron to the macrocycle, a 5 cm^{-1} shift of ν_2 band between low-spin $Fe^{II}TPP$ and $[Fe^{I}TPP]^-$ suggests that of only about ¼ of an electron of

the electron density was transferred to the macrocycle of porphyrin via back-bonding. Thus, most of the unpaired electron in $[FeTPP]^-$ resides in the metal-centered orbital (d_{z^2}), paired-electron density in the porphyrin e_g^* orbitals has been substantially increased relative to that present in the $Fe^{II}TPP$ complex.

Meanwhile, the β-substituted TPP complexes[16-17], $[FeTPP(CN)_4]^-$, $[FeTPP(CN)_3]^-$, $[FeTPPBr_4]^-$ have been reported to be π-anion radicals ($[Fe^{II}\text{-}P\cdot]^-$) by EPR spectroscopy[14]. And it showed that the electron-withdrawing groups like -CN, -Br at the β-pyrrole positions primarily stabilized the porphyrin e_g* orbitals[18], which would serve as the redox orbitals for macrocycle-centered reductions.

However, axial ligands like -Cl, -Br in $Fe^{III}(TPP)X$ primarily destabilize the metal d_{z^2} orbital which could serve as the redox orbitals for a metal-centered reduction. This suggests that the substituent groups can dramatically influence the electron distribution in the Fe^{II}-P reduction process. The fact is the one-electron reduction products of the series of $Fe^{II}(TPP)$ are influenced mostly by the presence of electron-withdrawing groups on the macrocycle. The explanation for the effect of the β-substituents and the axial ligands will be discussed later in this section.

1-2-2. Reduction of iron octaethylporphyrin complexes

The reduction of $Fe^{III}OEPCl$ is one of the most studied porphyrin systems besides $Fe^{III}TPPCl$. The structure of $Fe^{III}OEPCl$ shown in Figure 1-7[22] shows us that the iron is out of the plane by 0.50 Å. The reduction stage can be described as:

$$Fe^{III}(OEP)Cl \overset{+e}{\Rightarrow} Fe^{II}(OEP) \overset{+e}{\Rightarrow} [Fe(OEP)]^-$$

A number of spectroscopic techniques and physical measurements[13, 14, 20, 21], such as electron paramagnetic resonance (EPR), ultraviolet/visible spectroscopy (UV-vis), Mössbauer, nuclear magnetic resonance (NMR), Fourier transform infrared spectroscopy (FT-IR), electrochemistry, X-ray crystallography, and resonance Raman spectroscopy have been used in an effort to characterize the system. Resonance Raman (RR) spectroscopy has been a useful tool in the studies of heme proteins[19] and metalloporphyrins[20-21]. RR has been primarily used to measure the properties of the porphyrin macrocycle. Some of the RR lines serve as a sensitive indicator of the electronic state, the coordination number, or the core size of iron porphyrins.

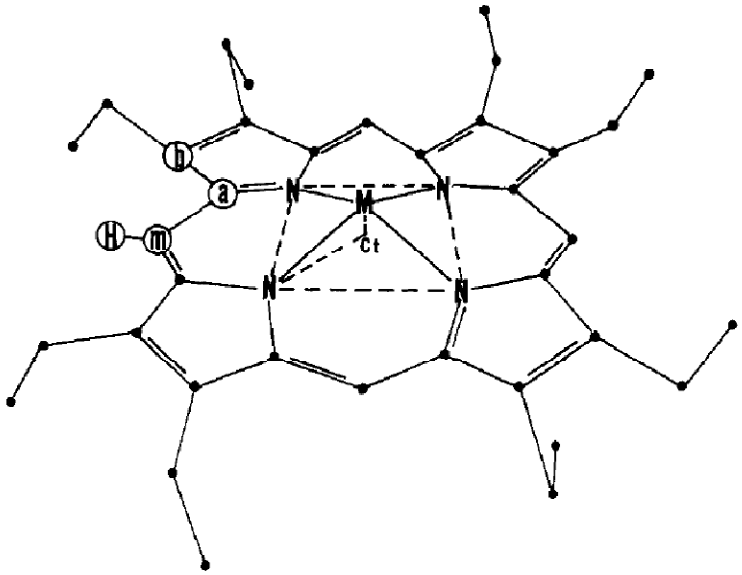

Figure 1-7. Labeling scheme for the porphinato (MOEP) moiety[22] (when M=$Fe^{III}Cl$, the distance of metal from porphyrin plane is 0.50 Å)

The changes of the UV-visible spectra of Fe^{III}(OEP)Cl to Fe^{II}(OEP) and the changes of B bands of Fe^{II}(OEP) to $[Fe(OEP)]^-$ are shown in Figure 1-8[14]. We can see the absorption peaks (wavelength/nm) are 372, 400, 502, 529, 630 for Fe^{III}(OEP)Cl; the absorption peaks (wavelength/nm) of B bands are 407, 458 for Fe^{II}(OEP); the absorption peaks (wavelength/nm) of B bands are 373, 419 and 455 for $[Fe^{I}(OEP)]^-$.

The resonance Raman of the Fe^{III}OEPCl, Fe^{II}OEP and $[FeOEP]^-$ with λ_{ex} at 441.6 nm by Kitagawa[14] are shown in Figure1-9. The ν_4, ν_3 and ν_{10} modes (cm^{-1}) are summarized in Table 1-2 for Fe^{II}OEP and $[FeOEP]^-$ in THF solution at room temperature.

Table 1-2. The resonance Raman frequencies of iron octaethylporphyrin complexes (λ_{ex} =441.6 nm)

Frequency Modes	Fe^{II}OEP	$[FeOEP]^-$ (300K)
ν_{10} (cm^{-1})	1637, 1607	1568
ν_4 (cm^{-1})	1363	1364
ν_3 (cm^{-1})	1475	1492

For Fe^{II}OEP, on the basis of the ν_{10} frequencies[23-28], 1637 and 1607 cm^{-1}, the complexes are categorized as four coordinate intermediate-spin ferrous porphyrins and five-coordinate high-spin states ferrous porphyrins respectively. However, the pure ferrous intermediate-spin complex provides much more intense peaks at ν_{10} line. Therefore, the low intensity of the peak at ν_{10} line in Figure1-9 (B) suggests that the five-coordinate high spin state ferrous porphyrin is the major product. Meanwhile, the ν_3 band

at 1475 cm^{-1} is also within the category of the five-coordinate high spin states ferrous porphyrins from Kitagawa[26]. Thus, the main component of the first reduction product $Fe^{II}OEP$ in the THF solution should adopt the high spin five-coordinate structure designated as $Fe^{II}(OEP)(THF)$.

From Spiro[23] and Kitagawa[24-25], we know that the ν_4 line, which appears in the 1350-1375 cm^{-1} region, reflects the number of metal d_π electrons. An increase of metal d_π electron density will result in the decrease of ν_4 frequencies. The effect of d_π electrons on the ν_4 frequency can be understood because, if the number of metal d_π orbital increases, it will result an increase of delocalization to the porphyrin π^* orbitals (e_g), which are antibonding with respect to C_a-N bond[29] (Figure 1-7). Thus, the C_a-N stretching force which determines the ν_4 frequency[30] will decrease.

In Figure 1-9 (C) and (D), the resonance Raman of the $[FeOEP]^-$ was obtained at room temperature and at 77 K in THF solution with 441.6 nm excitation. In the frozen state, Raman lines at 1568, 1387 and 1492 cm^{-1} become weaker, but new lines appear at 1602, 1590 and 1497 cm^{-1}. Since the large spectral change upon freezing seems compatible with the spin transition from high to low states upon freezing, as reported by Cohen et al[31], Kitagawa concludes that at the room temperature, the reduced product $[FeOEP]^-$ is high spin.

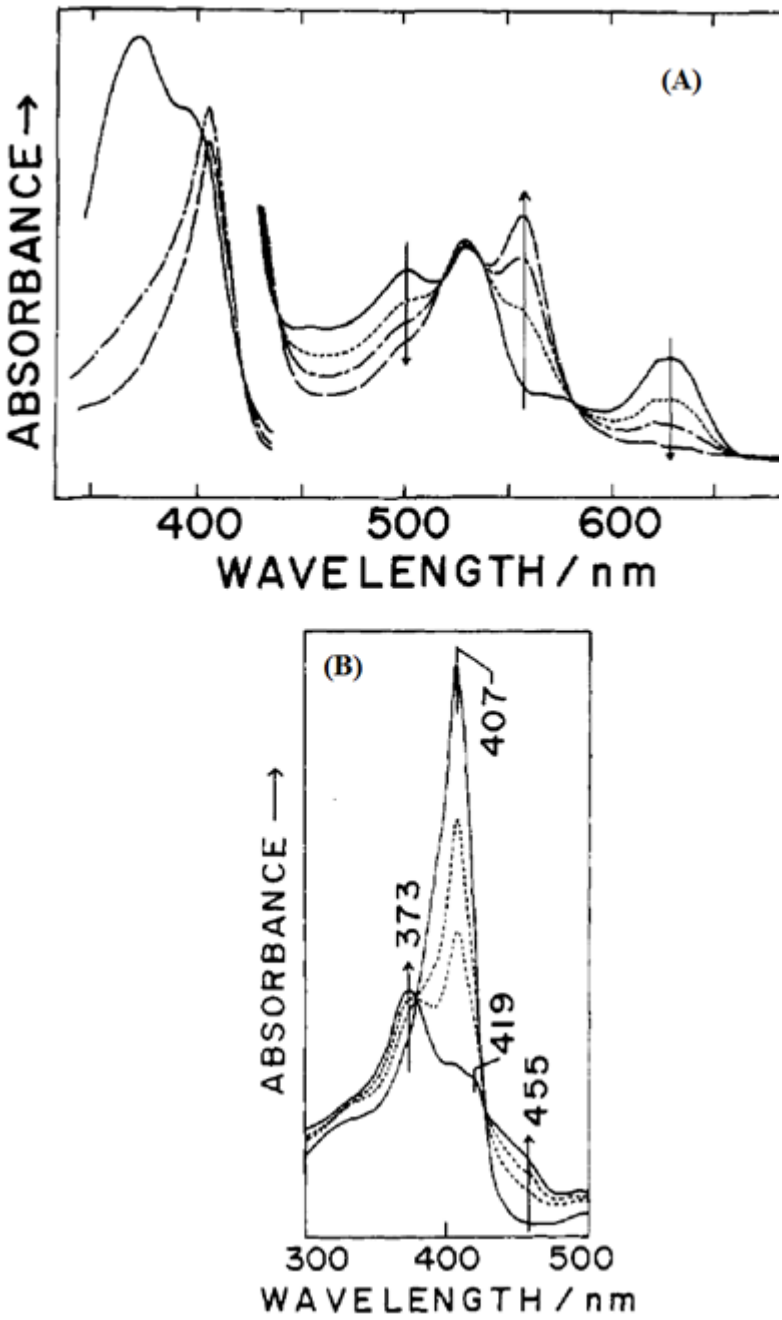

Figure 1-8[32]. The UV-visible spectra of iron octaethylporphyrin complexes
(A) Changes of the visible absorption spectra of first reduction of Fe^{III}(OEP)Cl to Fe^{II}OEP in THF; (B) Changes of absorption spectrum in the Soret region upon reduction from Fe^{II}(OEP) to $[Fe(OEP)]^-$ in THF.

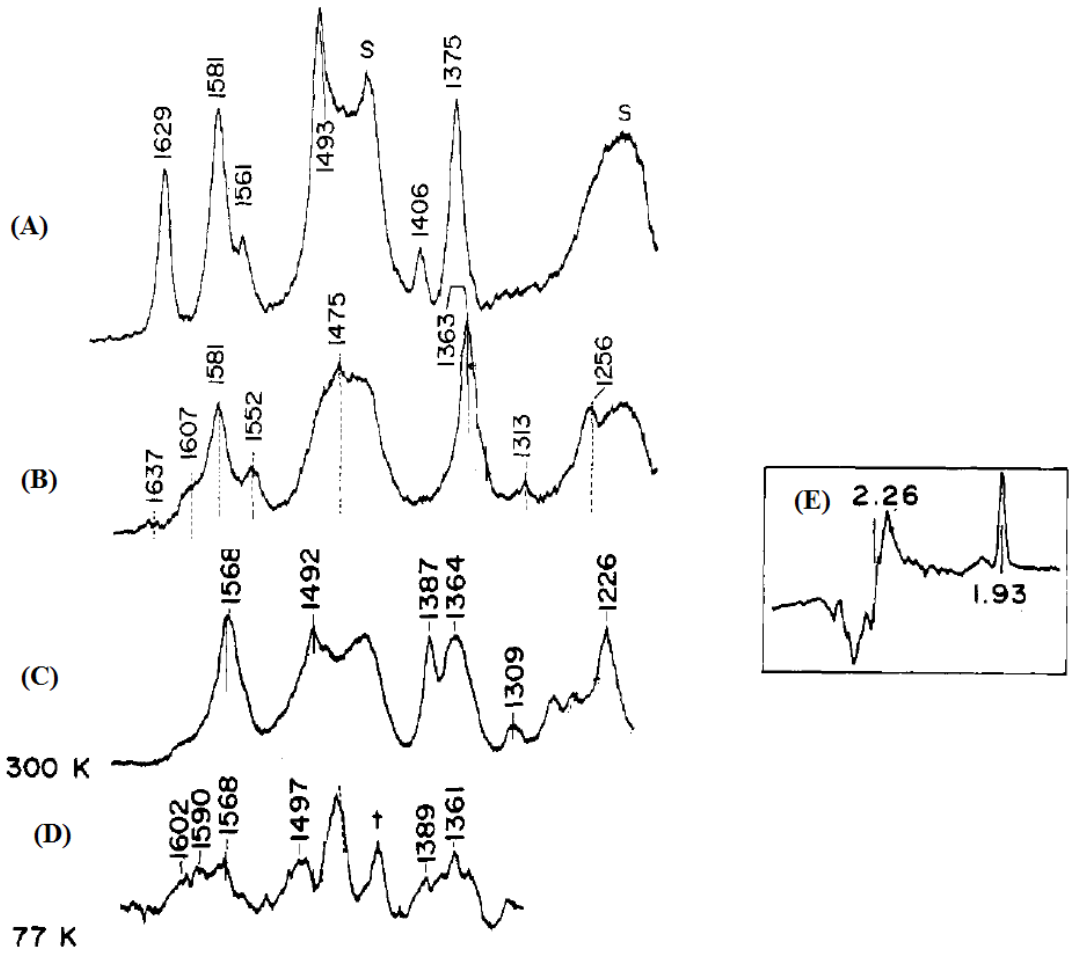

Figure 1-9[14]. The Raman and EPR spectra of iron octaethylporphyrin complexes in THF solution (λ_{ex} = 441.6nm)[34]: (A) Fe^{III}(OEP)Cl; (B) Fe^{II}(OEP); (C) $[Fe(OEP)]^-$ at room temperature, 300K; (D) $[Fe(OEP)]^-$ at 77K. (E) EPR spectrum of $[Fe(OEP)]^-$ at 77K in THF solution

In Figure 1-9 (E), the EPR spectrum of $(FeOEP)^-$ gives peaks at $g_\perp$=2.26 and $g_\parallel$=1.93 indicating the formation of the Fe^I porphyrin, which is expected to yield the EPR signals of $g_\perp$=2.30 and $g_\parallel$=1.93 from Cohen[31]. Thus, Kitagawa concluded that the reduction occurred at the d orbital of iron instead of the π orbital of porphyrin, leading to the iron(I) formulation as the reduced product. Based on the Raman and EPR spectra, Kitagawa concluded that the reduction product of $Fe^{II}(OEP)(THF)$ is $[Fe^IOEP]^-$ with high spin state.

However, the conclusion of the high spin state is incompatible with both the room temperature ^2H paramagnetic shifts and magnetic moment determined for $[Fe^IOEP]^-$ by Hickman[33]. Bocian also confirmed that the $[Fe^IOEP]^-$ exhibit a low-spin configuration at room temperature by ^1H NMR. Thus Kitagawa's conclusion about the high-spin formulation is incorrect. The reduction stages of the iron(III) octaethylporphyrin can be described as:

$$Fe^{III}(OEP)Cl \overset{+e}{\Rightarrow} \underset{(\text{high spin})}{Fe^{II}(OEP)(THF)} \overset{+e}{\Rightarrow} \underset{(\text{low spin})}{[Fe^{I}(OEP)]^-}$$

Conclusion of the two electron reduced iron tetraphenylporphyrin (TPP) and octaethylporphyrin (OEP) systems:

As discussed above, two electron reduced iron porphyrins can assume several electronic structures upon the introduction of electron- withdrawing substituents on the porphyrins. The electron-withdrawing substituent on the porphyrin ring can cause two effects. One is to decrease the energy level of the porphyrin e_g orbital shown in Figure 1-10[14]. It shows that the Fe(II) porphyrin e_g level decreases due to the electron withdrawing groups. The other effect is a weakening of the interaction between the iron and the porphyrin due to a decrease in the electron density at the pyrrole nitrogen of the porphyrin ring. According to these effects, the electron structures of the two electron reduced iron porphyrin complexes can be roughly classified into four types as shown in Figure 1-11[34].

In the case of iron porphyrins with weak electron withdrawing substituents (-Cl, -CHO, -Br etc.) on either OEP or TPP ligands, the energy level of the e_g orbitals are much higher than that of the d_{z^2} orbitals and there is strong ligation of the porphyrin ligands (Type I). Consequently, complexes of type I are Fe(I) porphyrin anion bearing no axial ligand.

If there is a stronger group, like one “-CN” on the OEP or TPP ring, it will result in a weaker ligation of the porphyrin to the central iron, forming five-coordinated Fe(I)

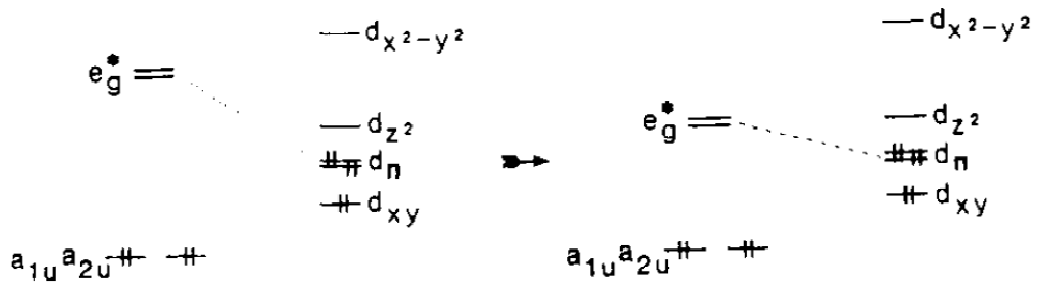

Figure 1-10. The effects of electron-withdrawing group on the orbital of low-spin Fe^{II} porphyrin system[14]

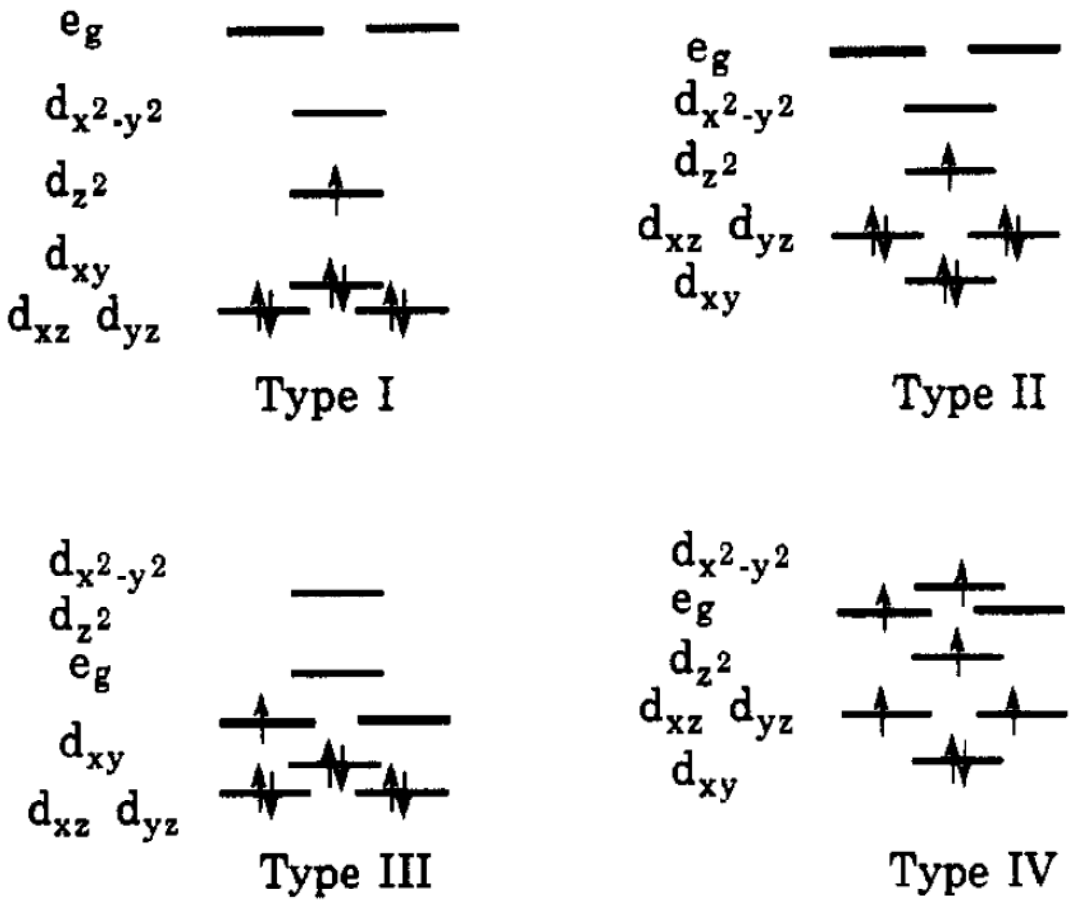

Figure 1-11. Four types of electronic structures of two electron reduced Iron(III) porphyrin complexes[34]:
Type I: four coordinated iron(I) low spin porphyrin;
type II: five coordinate iron(I) low spin porphyrin;
type III: four coordinate iron(II) low spin porphyrin anion radical;
type IV: five coordinated iron(II) high spin porphyrin anion radical.

species (Type II). When four strong electron withdrawing groups (-CN etc.) are added to the porphyrin ring, there will be a big decrease of the e_g level, which will become even lower than that of the iron d_{z^2} orbital. Thus, the unpaired electron occupies the e_g orbital instead of the d_{z^2} orbital (Type III). If the electron withdrawing groups (-NO_2 etc.) are much stronger, the e_g orbital level will become even lower, the five-coordinate Fe(II) porphyrin anion radicals will be produced (Type IV).

For Type III and Type IV, the unpaired electron isn't restricted to the e_g orbital but has different degrees of delocalization. Since the e_g orbitals have the same symmetry with d_{xz} and d_{yz}, the unpaired electron will delocalize to the d_{xz} and d_{yz} orbitals, depending on the energy gap. For a complex of type III, the structure will be a resonance hybrid between the iron(I) porphyrin anion with the iron(II) π radical anion, which is:

$$Fe^{I}P^{-} \leftrightarrow (Fe^{II}P\cdot)^{-}$$

For a complex of type IV, since the energy gap between e_g orbital of porphyrin and the d_{xz} and d_{yz} orbitals of metal is much bigger, the delocalization will be very weak and can even be ignored. The structure of the reduced product of type IV will mostly be the iron(II) π radical anion $(Fe^{II}P\cdot)^{-}$.

1-3. Iron porphinone complexes

The structure[35] of iron(III) porphinone chloride Fe^{III}(OEPone)Cl is shown in Figure 1-12, 1-13 and 1-14. Two types of Fe-N distances are observed in Fe^{III}(OEPone)Cl: "short" Fe-N distances to the three pyrroles [Fe-N (1), Fe-N (2), Fe-N (3) in Figure 1-13 (a)] range from 2.058(4) to 2.066(4) Å and a "longer" Fe-N distance [Fe-N (4) in Figure 1-13 (a)] at 2.125(5) Å to the pyrrolinone ring. The macrocycles of Fe^{III}(OEPone)Cl have a saddled conformation. The iron atom is displaced 0.46 Å out of the plane of the macrocycle and the axial Fe-Cl distances is 2.217 Å. These bond distances are comparable to those high-spin penta-coordinate iron(III) porphyrin, such as Fe^{III}TPPCl[12,36] which is 0.47 Å out of the plane and the axial Fe-Cl distance is 2.211(1) Å. The pyrrolinone ring of Fe^{III}(OEPone)Cl has a lengthened C_β-C_β bond at 1.507 Å because of the saturation of the ring. The C_α-C_β bond containing the oxo-substituent is shorter than the C_α-C_β bond containing the *gem*-diethyl group [C_α-$C_{\beta(oxo)}$ at 1.479(8) Å versus C_α-$C_{\beta(gem\text{-}diethyl)}$ at 1.514(8) Å], which suggests that the keto group is conjugated with the π system of the macrocycle.

In Figure 1-14 (a), a striking feature of the structure of Fe^{III}(OEPone)Cl is that all ethyl groups, except one *gem*-diethyl group, are on one side of the molecule with the single axial ligand. This type of structural feature is indicative[36] of minimal inter-ring π–π interactions. Figure 1- 14 (b) shows a top-down view of an inversion-related pair of rings. For the two iron centers, they are separated by 7.77 Å with a mean plane

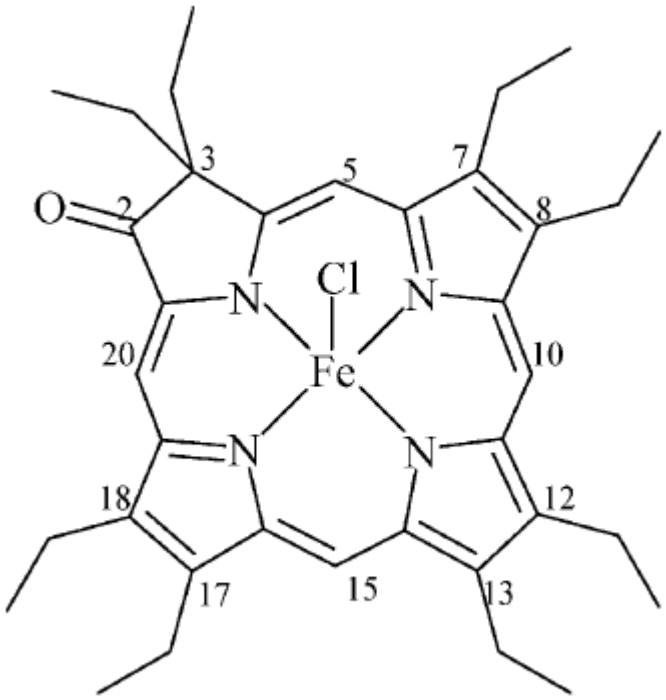

Figure 1-12. The structure of iron(III) β-oxooctaethylporphinone chloride [Fe^{III}(OEPone)Cl]

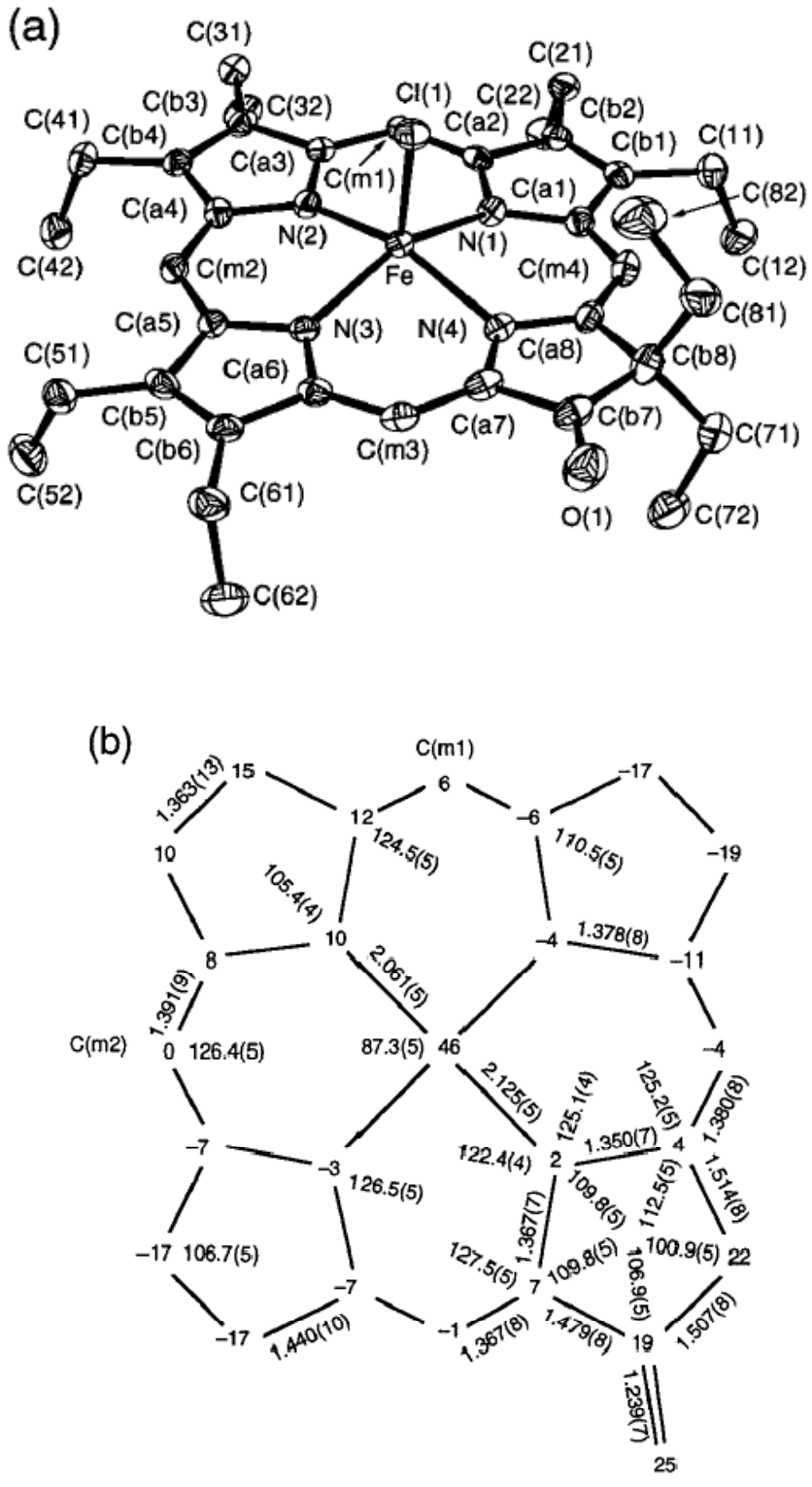

Figure 1-13. Structure of $Fe^{III}(OEPone)Cl^{35}$ (continued). (a) Labeled ORTEP diagram (b) Formal diagram giving the perpendicular displacements of each atom from the 24-atom mean plane of macrocycle (in Å $\times 10^2$)

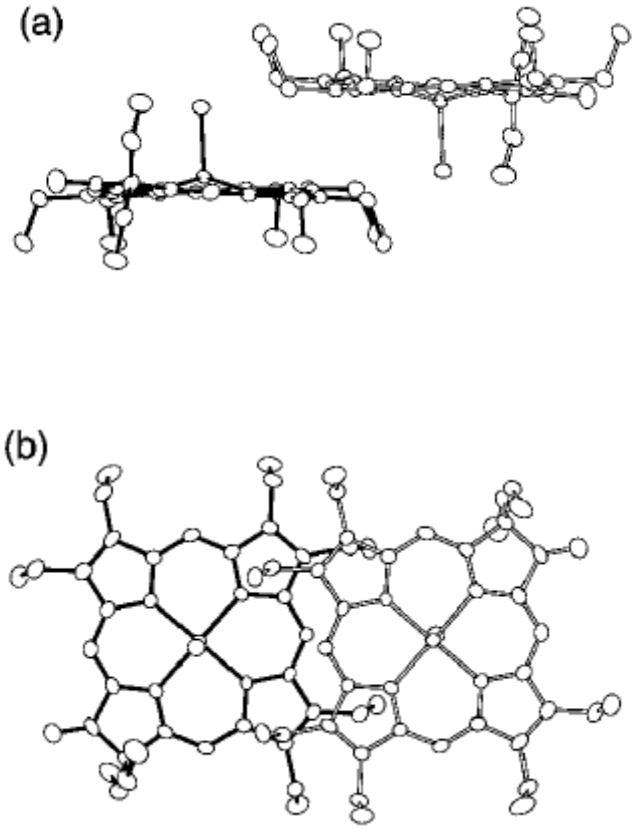

Figure 1-14. Structure of Fe^{III}(OEPone)Cl^{35} (continued). (a) Edge-on view and (b) top-down views of the closest inversion related dimeric unit of Fe^{III}(OEPone)Cl

separation of 3.39 Å. Thus, the dimeric Fe^{III}(OEPone)Cl unit has no direct overlap and has an "edge-to-edge" orientation.

Figure 1-15 shows the visible spectra obtained during the first and second reductions of Fe^{III}(OEPone)Cl in THF by OTTLE (Optically Transparent Thin-Layer Electrode) spectroelectrochemisty[37]. Spectral information referred to Figure 1-15 are summarized in Table 1-3. The addition of the first electron led to a red-shift (13 nm) and an increase in absorbance of the Soret bands. The addition of the second electron into Fe^{II}(OEPone) led to a dramatic change in both Soret and visible regions with decreased and broadening of Soret bands, and a red-shift of the visible bands (wavelength/nm) from 594 to 645.

Table 1-3. UV-visible spectra of iron porphinone complexes[37]

Compounds	solvent	λ_{max} (nm)
Fe^{III}(OEPone)Cl	THF	386, 400, 482, 546, 596, 658, 730
Fe^{II}(OEPone)	THF	399, 413, 486, 545, 595, 661
$[Fe(OEPone)]^-$	THF	364, 407, 446, 522, 585, 645

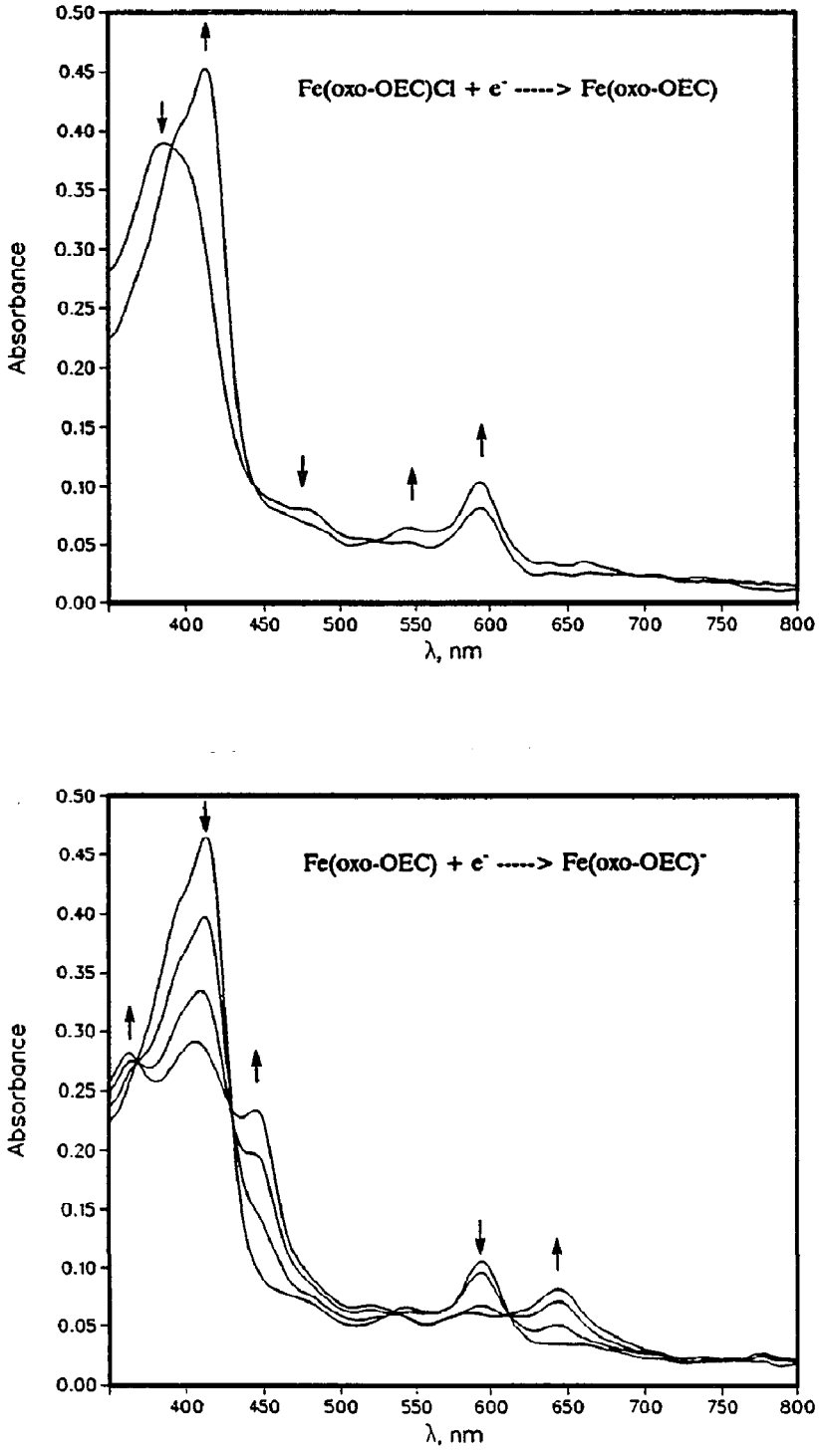

Figure 1-15. Visible spectra obtained during the first (top) and second (bottom) reductions of Fe^{III}(OEPone)Cl in THF by OTTLE spectroelectrochemisty[37]

The infrared spectra shown in Figure 1-16 were obtained in the matrix of THF-d_8 by Wei[38] and the data are summarized in Table 1-4 below.

Table 1-4. Infrared spectroelectrochemistry of iron porphinones[38]

Compounds	ν_{CO} (cm^{-1})	other infrared bands (cm^{-1})
Fe^{III}(OEPone)Cl	***1719***	1563, 1536, 1383, 1268, 1228, 1221, 1209, 754, 732
Fe^{II}(OEPone)	***1703***	1550, 1530, 1361, 1221, 754, 742
[Fe(OEPone)]$^-$	***1671, 1578***	1609, 1548, 1526, 1361, 1219, 728

For the first reduction $Fe^{III}(OEPone)Cl \overset{+e}{\Rightarrow} Fe^{II}(OEPone) + Cl^-$, the most noticeable change is that ν_{CO} shifted from 1719 cm^{-1} to 1703 cm^{-1}, which indicates a weakening of the macrocycle carbonyl band. This is probably due to the increased electron density on the porphyrin ring. Since the back-bonding from Fe(II) is stronger than that of Fe(III) to the porphyrin, the electron density increased in the first reduction product Fe^{II}(OEPone).

Upon further reduction $Fe^{II}(OEPone) \overset{+e}{\Rightarrow} [Fe(OEPone)]^-$, the ν_{CO} shifted largely from 1703 cm^{-1} to 1671cm^{-1}, indicating a further weakening of the porphinone carbonyl group. As the carbonyl vibration is shifted to lower energy, the coupling between the ring and the carbonyl may happened thus result the split of the carbonyl vibration. DFT calculation by Wei[38] shows that the carbonyl mode becomes more coupled with the ring vibrations when shifted to a lower energy.

Thus, the reduction of iron in iron porphinones can be observed in changes in the carbonyl infrared band. The carbonyl vibrations are quite sensitive to the interaction between the central metal and the porphinone ring. When ferric porphinones were reduced to ferrous complexes, the ν_{CO} band decreased by 16 cm^{-1}. This downshift is because of the increased back-bonding from the iron(II) orbital to the porphinone orbital compared to iron(III). Further reduction of Fe(II) porphinone cause a dramatic downshift by 32 cm^{-1} also a split of the ν_{CO} bands due to the carbonyl vibration's coupling with the porphyrin ring vibrations when at lower energy. Thus, the use of FTIR spectroelectrochemistry combination with DFT calculation is shown to be valuable in Wei's studies of the reduction of iron porphinone.

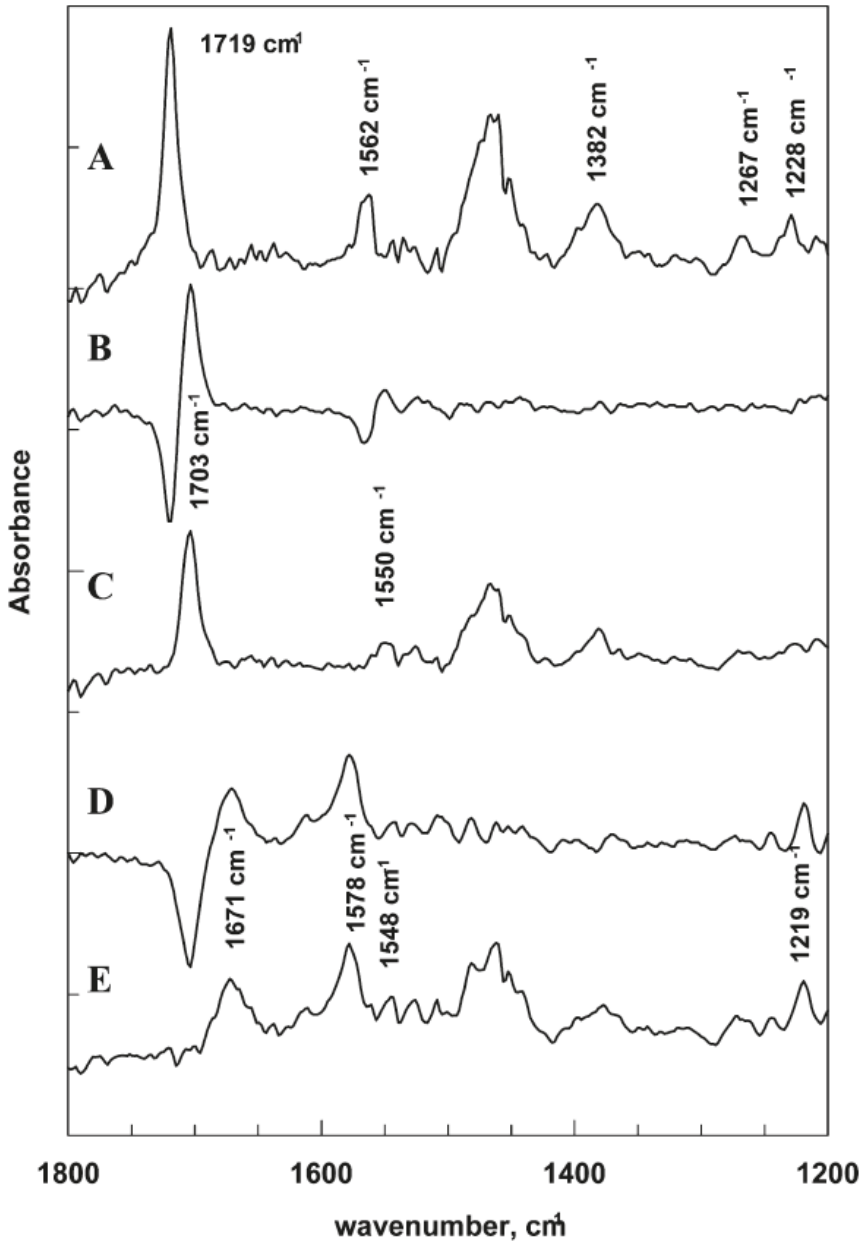

Figure 1-16[38]. FT-IR spectra of iron porphinone complexes in THF-d_8 matrix (A) FTIR spectrum of Fe^{III}(OEPone)Cl; (B) FTIR difference for Fe^{II}(OEPone) and Fe^{III}(OEPone)Cl; (C) FTIR spectrum of the one electron reduction product, Fe^{II}(OEPone); (D) FTIR difference of $[Fe(OEPone)]^-$ and Fe^{II}(OEPone); (E) FTIR spectrum of the two electron reduction product, $[Fe(OEPone)]^-$. Spectra A, C, and E are solvent subtracted. Solvent: THF-d_8; electrolyte: TBAP.

1-4. Aim of this work: Synthesis and reduction of the iron(III) porphinone complexes and their spectroscopy studies

To date, only $[FeTPP]^-$ (TPP = tetraphenylporphyrin) and $[FeOEP]^-$ (OEP = octaethylporphyrin) and their derivatives have been examined in comparable detail[33,39-40]. However, much less work has been done on the free base porphinone and metal porphinone complexes.

Porphinones, a third class of tetrapyrrole, have been viewed as the analogues of hydroporphyrins. The proposed analogy between porphinones and hydroporphyrins was based upon the similarity of the UV-visible spectra of the two classes of macrocycle[41]. However, recent investigations have established that the redox potentials of porphinones are distinctly different from those of either porphyrins or hydroporphyrins[42-43]. These observations imply that porphinones may have unique electronic structures.

The differences can be also found during the reduction of the iron(III) porphyrin and porphinone complexes. For comparing the reduction of Fe^{III}(OEPone)Cl with that of Fe^{III}TPPCl and Fe^{III}OEPCl, the half wave potentials[48, 49] are summarized in Table 1-5. In Table 1-5, we can see $E_{1/2,1}$ value of Fe^{III}(OEPone)Cl (-0.35V) are 100mV, 227 mV positive of Fe(OEP)Cl (-0.45V) and Fe^{III}(TPP)Cl (-0.577V). The $E_{1/2,2}$ value of Fe(OEPone)Cl (-1.23V) are 30mV and 212mV positive of Fe^{III}(OEP)Cl (-1.26V) and Fe(TPP)Cl (-1.442V) respectively. As expected, the $E_{1/2,1}$ and $E_{1/2,2}$ values shift in the negative direction as the porphyrin ring becomes more saturated, which also prove that

the presence of the keto group on the ring make it harder for the reduction.

$$Fe^{III}(P)Cl + e^- \rightarrow Fe^{II}(P) + Cl^- \quad (1) \quad E_{1/2,1}$$

$$Fe^{II}(P) + e- \rightarrow [Fe(P)]^- \quad (2) \quad E_{1/2,2}$$

Table 1-5. Half-wave potential for the reduction of iron porphyrin and porphinone complexes

Complex	Solvent	$E_{1/2,1}$ (V) ($Fe^{III}P/Fe^{II}P$)	$E_{1/2,2}$ (V) ($Fe^{II}P/[Fe^{I}P]^-$)	Ref.
Fe(OEP)Cl	THF	-0.45[a]	-1.26[a]	48
Fe(TPP)Cl	THF	-0.577[a]	-1.442[a]	49
Fe(OEPone)Cl[b]	THF	-0.35[a]	-1.23[a]	48

a. Data were obtained versus $Ag/AgNO_3$ reference electrode.
b. For comparison to the literature values[48], 0.456 V was subtracted from the data of Fe^{III}TPPCl to obtain values versus SCE.

In most of the porphyrin studies, highly reduced metalloporphyrins have been prepared by electrolytic reduction[31, 45-46], some have been generated in clean conditions by the sodium mirror contact technique[39] or sodium anthracenide reduction[13] method. It has been proven that the sodium anthracenide reduction method is more efficient than electrolytic reduction since the electrolysis often produced undesirable byproducts. In this work, the sodium anthracenide reduction method will be used to reduce the iron(III) porphinone chloride.

Previously, the reduction of Fe^{III}(OEPone)Cl have been studied by OTTLE spectroelectrochemistry [44] and infrared spectroelectrochemistry[47] in our lab. Infrared spectroscopy is ideally suited to investigate the structure of free base and metal porphinone complexes because they have ketone groups on the porphyrin rings. The υ_{co} band in the ring of porphinone in the infrared spectra is significantly stronger than most of the porphyrin ring vibrations, making it easy to observe. The infrared spectra of metalloporphyrins [48-51] and porphinediones[52] have both been studied in considerable detail.

However, resonance Raman spectroscopy, which is a powerful tool to study the porphyrin structures and the electron densities hasn't been done yet. The reduction product of iron(III) porphinone chloride will be characterized by UV-visible, infrared and Raman spectra in this work.

CHAPTER TWO

EXPERIMENT

2-1. Instrument

The UV-visible spectra were recorded on a Hewlett-Packard 8452A diode array spectrophotometer. It is a single-beam, microprocessor-controlled spectrophotometer, with a range from 190 nm to 820 nm with 2 nm resolution. The spectrophotometer is controlled from a computer equipped with the software of OlisGlobalWorks running on Windows XP.

The Proton-NMR data were obtained on a Varian Mercury-300 MHz spectrometer. Spectra were taken with the sample mixed in the CD_2Cl_2 or $CDCl_3$ (Aldrich) matrix in the NMR tubes.

The infrared spectroscopy data were obtained on the Thermo Nicolet Nexus 670 Fourier-transform infrared spectrophotometer. Spectra were taken from 4000 to 400 cm^{-1} with the sample mixed in the matrix of potassium bromide (KBr, Aldrich).

Resonance Raman spectroscopy was obtained by mixing the sample in the KBr matrix in tightly covered NMR tubes. The test conditions will be described separately when giving the resonance Raman spectrum of the specific porphyrin complexes in the Result and Discussion part.

2-2. Chemicals

The following reagents were purchased from Aldrich Chemical Company: free base tetraphenylporphyrin[H_2TPP], iron(III) tetraphenylporphyrin chloride [Fe^{III}(TPP)Cl], free base octaethylporphyrin (H_2OEP), octaethylporphyrin iron (III) chloride [Fe^{III}(OEP)Cl], and Tetrahydrofuran (THF).

Tetrahydrofuran was distilled by heating at reflux over sodium in a nitrogen atmosphere until the dark blue benzophenone anion color was persistent, and then stored in the glove box.

2-2-1. Synthesis of the free base porphinone (H_2OEPone) complex

Porphinone (H_2OEPone)[32, 59-61] was prepared by oxidation of H_2OEP via metal inserted purification. 2.8 g of H_2OEP was dissolved into 600 mL of CH_2Cl_2 containing 1% anhydrous pyridine. The solution was degassed for half an hour. To the solution was added 2 g of OsO_4 in 10 mL of anhydrous ether. The solution was stirred in dark at room temperature under nitrogen atmosphere for 24 hours, and then the reaction was stopped by adding 150 mL methanol and gassed 15 minutes of hydrogen sulfide (H_2S).

The solution was filtered and evaporated to obtain a residue. The residue was redissolved in 700 mL of methylene chloride, and then mixed with 20 mL of 70 % $HClO_4$. After the solution was stirred for 30 min, the mixture was washed with 600 mL distilled water for three times. A crude product (2.6 g) was obtained after evaporating the solvent and was a mixture of H_2OEPone, unreacted H_2OEP and a small amount of di- or tri-oxoporphinones.

Purification of the crude product was achieved by chromatography via their respective zinc complexes on an alumina column. To produce the zinc complexes[54], the crude products were put into a round bottom flask with zinc acetate dehydrate in $CHCl_3$/methanol (200 mL/100 mL) and heated to reflux for one hour. The reaction was stopped when the solution's color turned blue. The solution was rinsed with 300 mL distilled water three times when it cooled down. The solvent was removed and the purification was done on an alumina column. Elution was initiated with chloroform. A

small violet band containing H_2(2, 6-dioxo-OEBC), which did not react with zinc acetate eluted first (yield= 5 %). The UV-visible spectra in THF solution give the peaks[56] λ_{max} (wavelength/nm) at 346, 374, 464, 492, 568, 688, 728. The second band containing Zn(OEP) (pink, yield ≈ 40 %) was eluted with $CHCl_3$ containing 0.5% methanol. The UV-visible spectra in THF solution gave peaks[56] at λ_{max} (wavelength/nm) at 330, 406, 536 and 572. The third band was eluted with $CHCl_3$ containing 5% methanol, which contained Zn(OEPone) complex (blue, yield about 40%). UV-vis (THF) λ_{max} , nm (ε, $mM^{-1}cm^{-1}$): 402 (158), 486 (9.4), 506 (13), 542 (15), 586 (8.8), 614 (5.8), 642 (43); ^1H NMR ($CDCl_3$), δ: -2.90 (2H, NH), 0.34, 0.36, 0.39 (6H total, gem-CH_3); 1.80-1.89 (18H total, CH_3); 2.75 (4H total, gem-CH_2); 3.94 (×2), 4.04, 4.07, 4.09 (×2) (quartet, 2H, CH_2); 9.12, 9.83, 9.85, 9.94 (1H each, meso-H). H_2OEPone was obtained by washing with 10% HCl quantitatively. The UV-visible spectra (THF) λ_{max} , nm (ε, $mM^{-1}cm^{-1}$)[42]: 402 (158), 486 (9.4), 506 (13), 542 (15), 586 (8.8), 614 (5.8), 642 (43); Proton-HMR[42] ($CDCl_3$), δ : -2.90 (2H, NH), 0.34, 0.36, 0.39 (6H total, gem-CH_3), 1.80-1.89 (18 H total, CH_3); 2.75 (4H total, gem-CH_2), 3.94 (×2), 4.04, 4.07, 4.09 (×2) (quartet, 2H, CH_2); 9.12, 9.83, 9.85, 9.93 (1H each, meso-H).

2-2-2. Synthesis of iron (III) porphinone chloride

Synthesis of Fe^{III}(OEPone)Cl[57]: 25 mg of free base porphinone (H_2OEPone) was placed in 15 mL of acetic acid containing 40 mg sodium acetate and 25 mg sodium chloride in a 50 mL flask. After the solution was degassed with nitrogen for 30 min, 50 mg iron (II) acetate was added. The mixture was then heated to a gentle boil for one hour. The completion of the reaction was detected by the quenching of the bright fluorescence with a UV lamp. The solvent was removed under vacuum after the mixture was cooled. The residue was washed with distilled water several times. The product was then dissolved in benzene and lyophilized to give pure crystals.

2-2-3. Deuterium exchange of the free base porphinone complex

Deuteration of H_2(OEPone)[58]: A 250 mL round bottom flask was dried in the oven for half an hour and then was purged with nitrogen for 15 min. To the flask was added 0.1 mmol of H_2OEPone, followed by 8.4 mL dimethyl sulfoxide (DMSO-d_6). The resultant mixture was degassed with nitrogen for thirty minutes after adding 0.47 mL of tetrabutylammonium hydroxide (1 M in methanol).

The mixture was heated at 177 ^{o}C for 24 hours under a slow flow of nitrogen. After that, the reaction was quenched by adding 10 mL of 1 M HCl and 50 mL of chloroform to the round bottom flask. Then the organic layer was separated and washed with an aqueous solution of sodium hydrogen carbonate three times until no more effervescence was observed. A few grams of sodium sulfate were added to the chloroform solution to dry the residual water and then the solution was filtered. The chloroform was evaporated under nitrogen and the remaining water was removed in a vacuum desiccator at room temperature. The crude product was chromatographed on the alumina column with chloroform which was then evaporated under nitrogen gas. The purified sample was dried in a vacuum desiccator at room temperature.

2-2-4. Reduction of iron (III) porphyrins and porphinone complexes

Reduction of Fe^{III}TPPCl, Fe^{III}OEPCl and Fe^{III}(OEPone)Cl[40]: The reductant, sodium anthracenide was prepared by accurate weighing 3 mmol anthracene into a vial with a Teflon-lined cap and placed in the dry box 24 hours before it reacted with excess sodium metal in the double distilled THF (less than 15 mL). The solution was allowed to react for 24 hours with occasional stirring before it was decanted from the unreacted sodium and diluted to 15 mL making a 0.2 M solution. The solution was dark blue.

0.25 mmol Fe^{III}OEPoneCl (Fe^{III}OEPCl, Fe^{III}TPPCl) was dissolved into a 50 mL round bottom flask with 20 mL of distilled THF. 100- or 200-µL Microtrol syringe were used to transfer 3 mL of the dark blue sodium anthracenide solution to the stirred Fe^{III}OEPoneCl (Fe^{III}OEPCl or Fe^{III}TPPCl) solution above. After 30 min the solution was filtered and 80 mL heptane was added. The solution was set aside for precipitation for 24 hour and then was filtered to get the final products.

CHAPTER THREE

RESULTS AND DISCUSSION

3-1. UV-visible, infrared and proton NMR spectrum of the free base porphinone complexes

The oxidation of H_2OEP to $H_2OEPone$ is provided by Chang et al[62]. Osmium tetraoxide is used as the oxidant, which rearranges the free base porphyrin to the porphinone in strong acid solutions. The scheme reaction is shown in Figure 3-1.

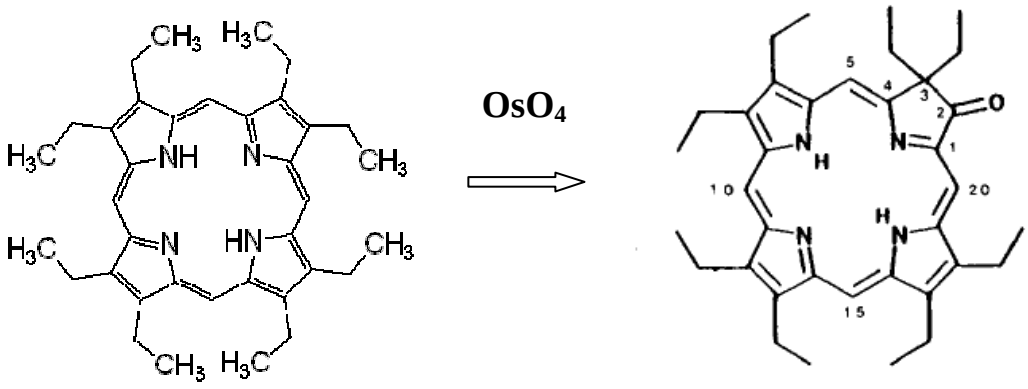

H_2OEP **$H_2OEPone$**

Figure 3-1 Scheme of the oxidation of H_2OEP to $H_2OEPone$

The UV-visible spectrum of the oxidization product $H_2OEPone$ (b) and the starting material H_2OEP (a) in THF solution are shown in Figure 3-2. After the oxidation, the Soret band has red-shifted (λ_{max}, wavelength/nm) from 398 to 406. The four peaks of $H_2OEPone$ (λ_{max}, wavelength/nm) at 406, 510, 548 and 642 are consistent with the literature results[42].

The IR spectrum of the oxidation product $H_2OEPone$ which shown in Figure 3-3 were

obtained in KBr matrix. The peaks (υ, cm^{-1}) are at 3335 (NH), 2963, 2932, 2872 (CH) and 1716(C=O). The results are consistent with the spectrum from Stolzenberg et al[42]. The IR spectrum of the starting material H_2OEP and the oxidation product $H_2OEPone$ are shown in Figure 3-4 (b) and Figure 3-4 (a) separately. For starting material H_2OEP, the strongest bands (υ, cm^{-1}) are at 1012 and1054. After the oxidation, these two bands still exist, and a new strong band at 1716 cm^{-1} due to υ_{CO} appears. We can see that the υ_{CO} of $H_2OEPone$ is comparably larger than the other porphyrin vibrations.

The proton NMR spectrum which shown in Figure 3-5 were obtained in CD_2Cl_2, the chemical shifts (δ, ppm) are summarized in Table 3-1. From Table 3-1, we can see the chemical shift positions of the oxidization product are consistent with the literature results from Stolzenberg[42]. From the integrated area, we use gem-CH_3 as the basis. Because there are 6H for gem-CH_3 in the molecule, there are about 4 meso-H, two N-H, about 6 H for gem-CH_2, about 15 H for -CH_2 and about 19 H for -CH_3 inside the molecule. The result fits the formulation of $H_2OEPone$.

The UV-visible, IR and proton NMR spectrum we have obtained are all consistent with that by Stolzenberg[42]. Thus, the oxidation product $H_2OEPone$ we have produced is the desired product.

Table 3-1. The proton NMR of H_2OEPone in CD_2Cl_2

Chemical shift δ (ppm)	integrate area	Proton Represented	Chemical shift δ (ppm) from Stolzenberg[42]
-2.95, -2.91 (singlet)	0.304 (2H)	-NH	-2.90, -2.85 (broad singlet)
0.38 (triplet)	0.999 (6H)	gem-CH_3	0.36 (triplet)
1.81~ 1.93 (multiple)	3.220 (19H)	-CH_3	1.81, 1.82, 1.84, 1.85, 1.86, 1.88 (triplet)
2.75 (multiple)	0.999 (6H)	gem-CH_2	2.75 (multiple)
3.95~4.11 (multiple)	***2.464 (14.78H)***	- CH_2	3.94× 2, 4.02, 4.06, 4.09× 2
9.22, 9.84, 9.95, 10.02 (singlet)	0.619 in total (4H)	meso-H	9.12, 9.83, 9.86, 9.94

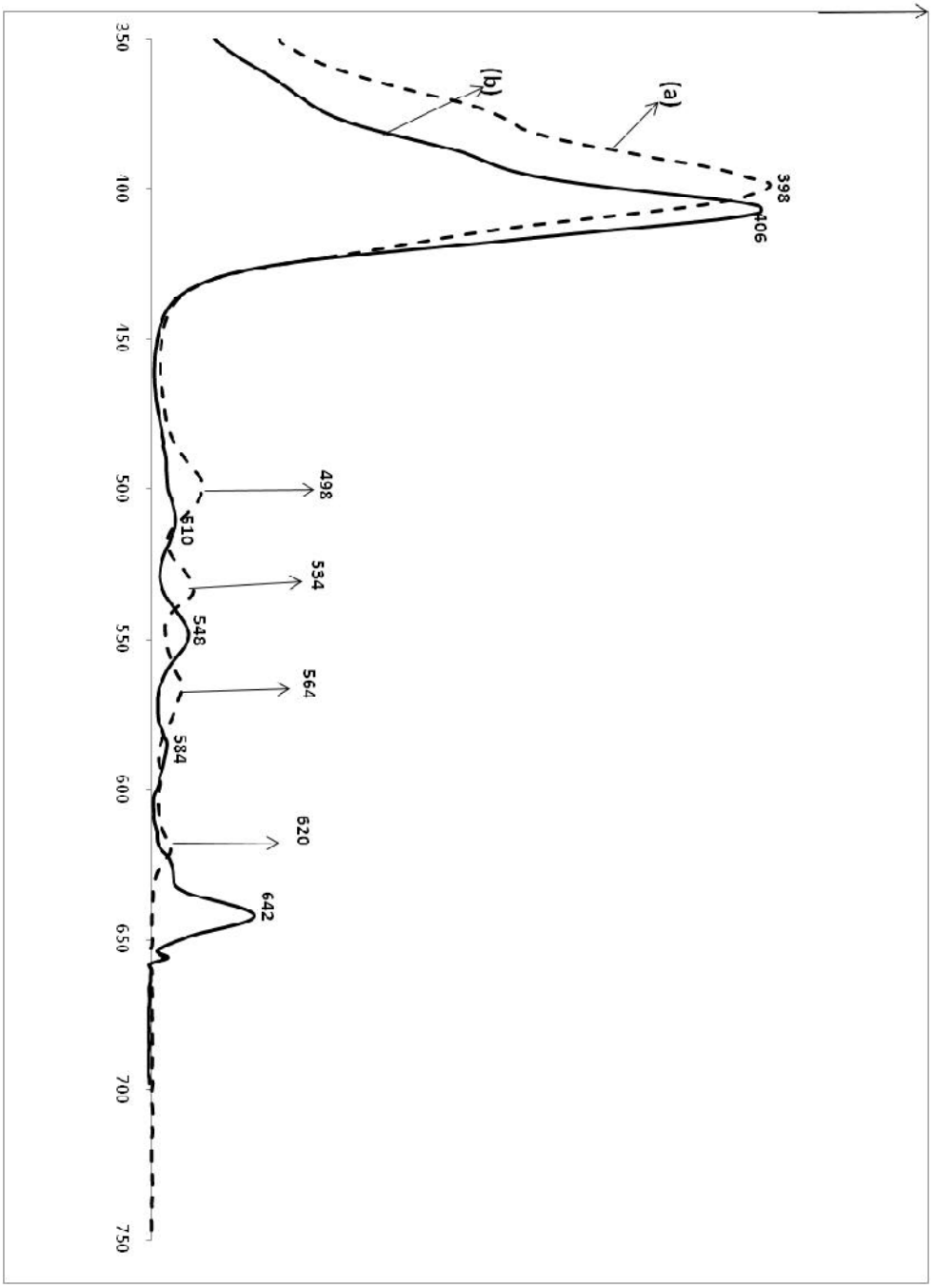

Figure 3-2. UV-visible spectrum of (a) H_2OEP (dash line) and (b) $H_2OEPone$ (solid line) in THF solution

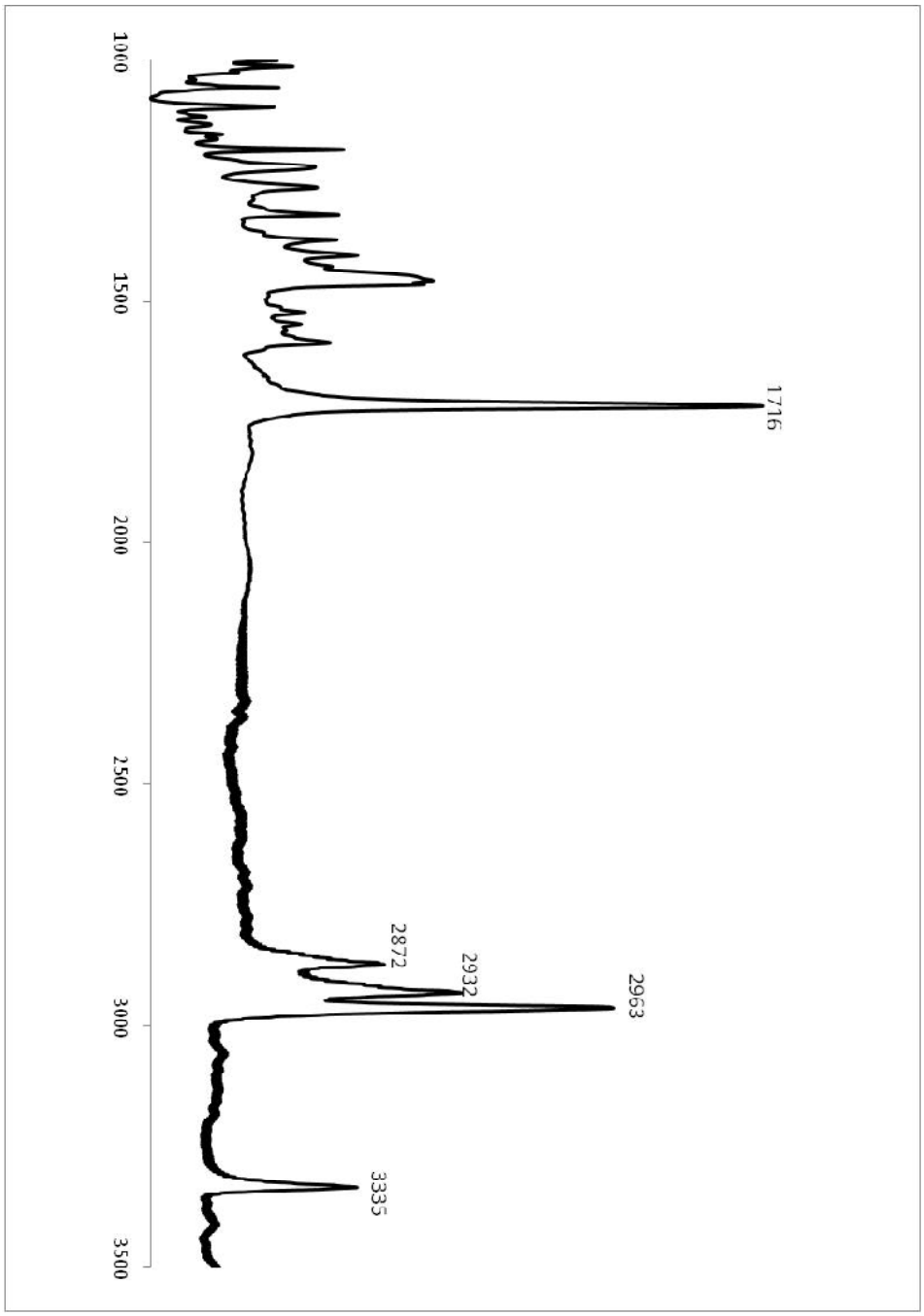

Figure 3-3. Infrared spectrum of H_2OEPone in KBr matrix

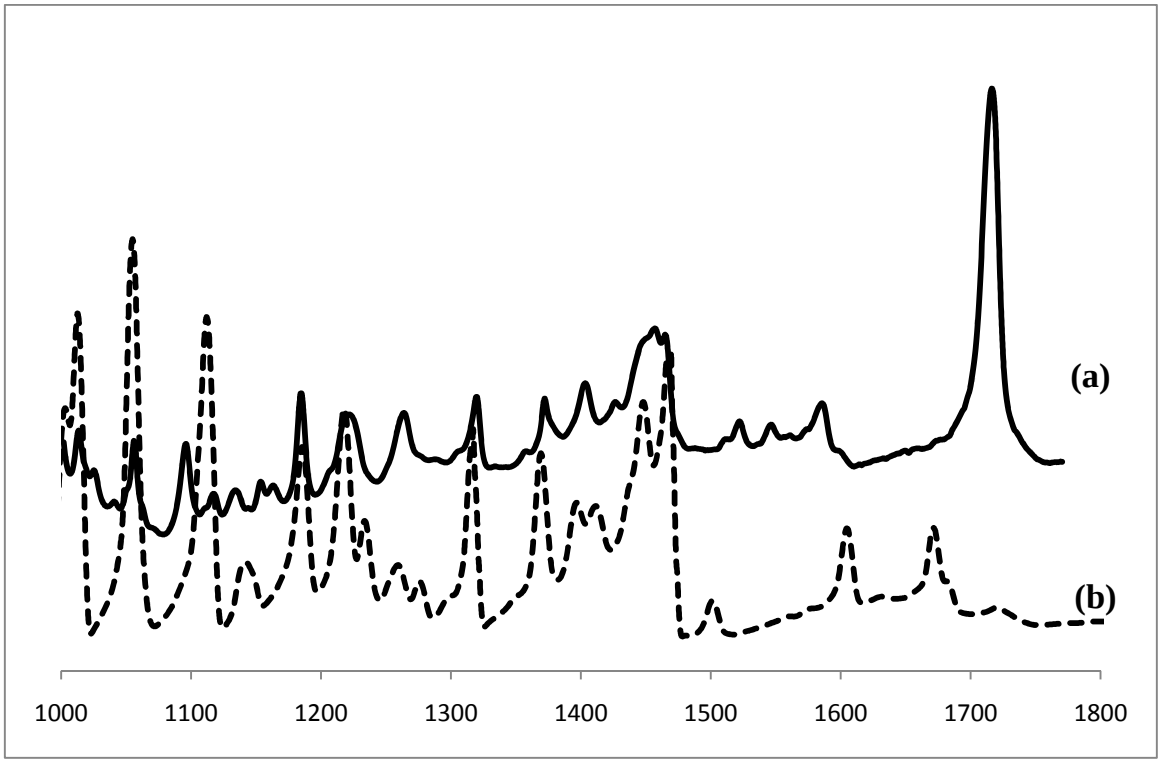

Figure 3-4. Infrared spectrum of (a) H_2OEPone (solid line) and (b) H_2OEP (dash line) in KBr matrix

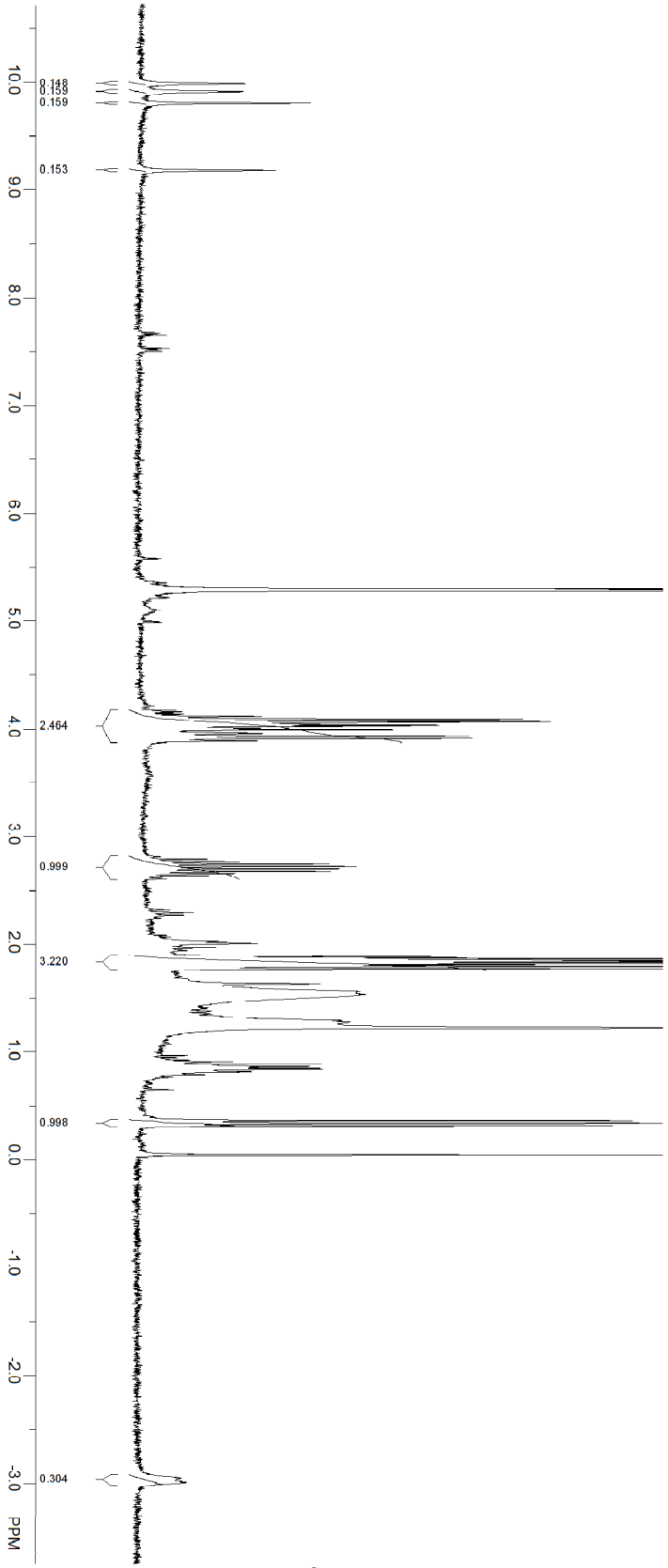

Figure 3-5. Proton NMR spectrum of H_2(OEPone) in CD_2Cl_2

3-2. UV-visible, infrared and proton NMR spectrum of the deuterated free base porphinone complex

Figure 3-6 shows the UV-visible spectrum of the starting material H_2(OEPone) and the deuterated product H_2(OEPone)-d_{12}[42]. The peaks (λ_{max}, wavelength/nm) of H_2(OEPone)-d_{12} at 406, 510, 548 and 642 are consistent with that of H_2(OEPone)[42]. After the deuteration, we had an identical spectrum which indicated that we had obtained the purified deuterated product without contamination.

The IR spectra of the starting material H_2OEPone and the deuteration product H_2OEPone-d_{12} shown in Figure 3-7 were obtained in KBr matrix. The FTIR spectra of H_2OEPone, H_2OEPone-d_{12} and their difference spectra are shown in Figure 3-8. There are three shifts in the difference spectra which are 1457 cm^{-1} to 1441 cm^{-1}, 1569 cm^{-1} to 1547 cm^{-1} and 1709 cm^{-1} to 1687 cm^{-1}. The downshifts of the vibration bands indicate a weakening of the bands which are due to the deuteration. ^{1}H have been deuterated to ^{2}D group, which increased the weight for the "C-proton" group, results a decrease of the vibration wavenumber.

The proton NMR spectra of the deuteration product H_2OEPone-d_{12} were obtained by the 300 MHz NMR spectrometer. Figure 3-9 shows the proton NMR of H_2OEPone-d_{12} in CD_2Cl_2. The chemical shifts δ (ppm) of H_2OEPone-d_{12} together with that of H_2OEPone are summarized in Table 3-2. From Table 3-2, we can see that the δ positions are almost unchanged during the deuteration, except the peak positions of "–CH_2", "gem-CH_2", "-

CH_3", "gem-CH_3" all shift slightly to the higher field. During the deuteration, the protons of "–NH" are gone. Thus, the deuteration rate of the proton of "–NH" is 100%. Another thing is that the protons of "–CH_2" left after the deuteration are only $\frac{0.701}{2.464} \times 100\% = 28.4\%$, making the deuteration rate 71.6%

Stolzenberg reported that the methylene positions were 90% deuteriated[42]. The result indicates that we have not achieved the literature results. We didn't pursue this further in our work, but, longer deuteration time may be needed to reach the 90% deuteration yield.

Table 3-2. The proton NMR of $H_2OEPone\text{-}d_{12}$ and $H_2OEPone$ in CD_2Cl_2

Chemical shift δ(ppm)		Integrate Area		Proton Represented
$H_2OEPone$	$H_2OEPone\text{-}d_{12}$	$H_2OEPone$	$H_2OEPone\text{-}d_{12}$	
-2.95, -2.91 (singlet)	none	0.304 (2H)	***None***	-NH
0.38 (triplet)	0.31(triplet)	0.999 (6H)	1.01 (6H)	gem-CH_3
1.81~ 1.93 (multiple)	1.72, 1.74, 1.77, 1.78, 1.80, 1.82	3.220 (19H)	3.375 (20 H)	-CH_3
2.75 (multiple)	2.68 (multiple)	0.999 (6H)	0.728 (4.36H)	gem-CH_2
3.95~4.11 (multiple)	3.90, 3.93, 3.99, 4.02	***2.464 (14.78H)***	***0.701(4.21)***	- CH_2
9.22, 9.84, 9.95, 10.02	9.22, 9.83, 9.96, 10.04	0.619 in total (4H)	0.675 in total (4H)	meso-H

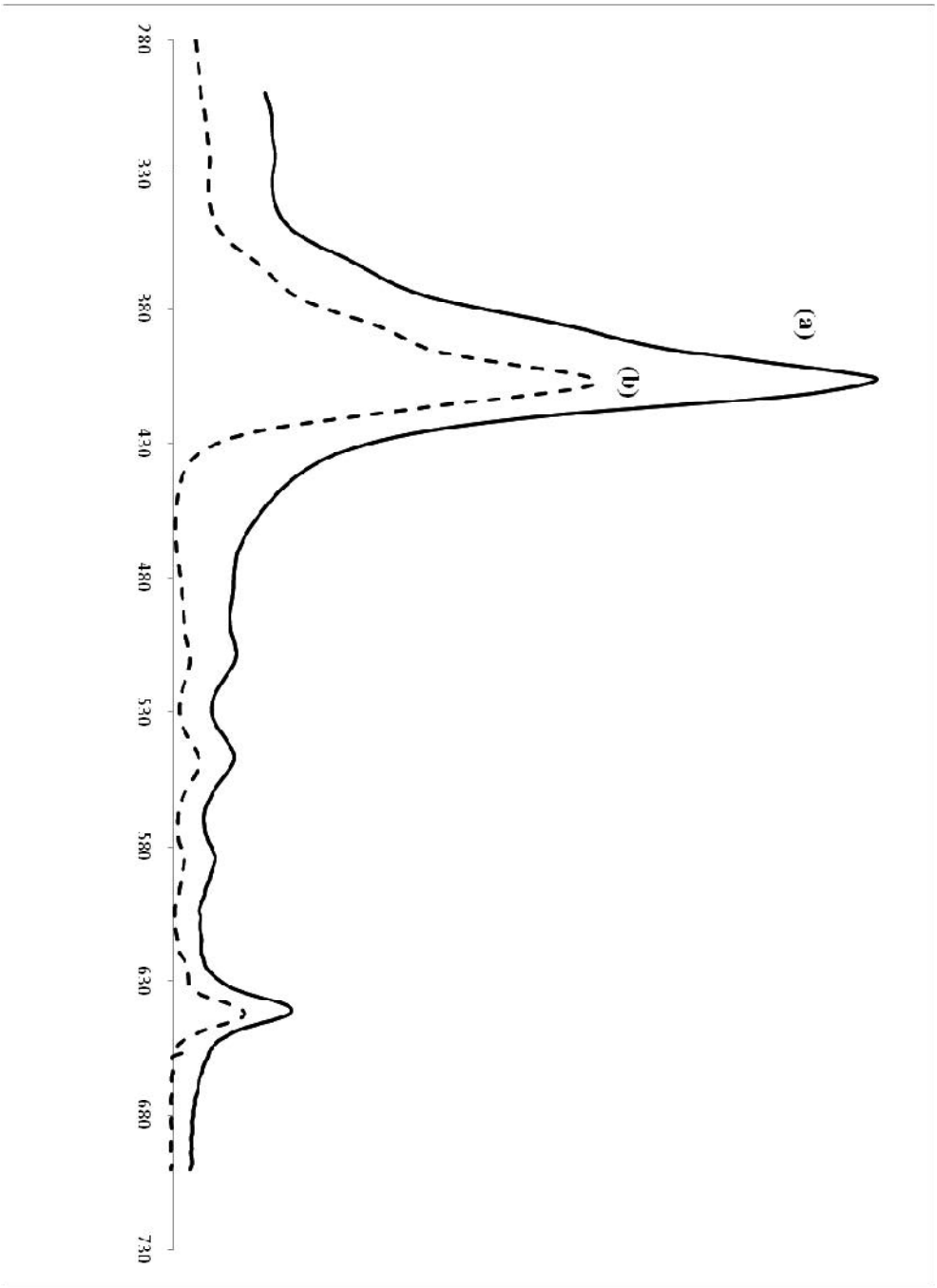

Figure 3-6. UV-visible spectrum of (a) H_2OEPone (solid line) and its deuteration product (b) H_2OEPone-d_{12} (dash line) in THF solution

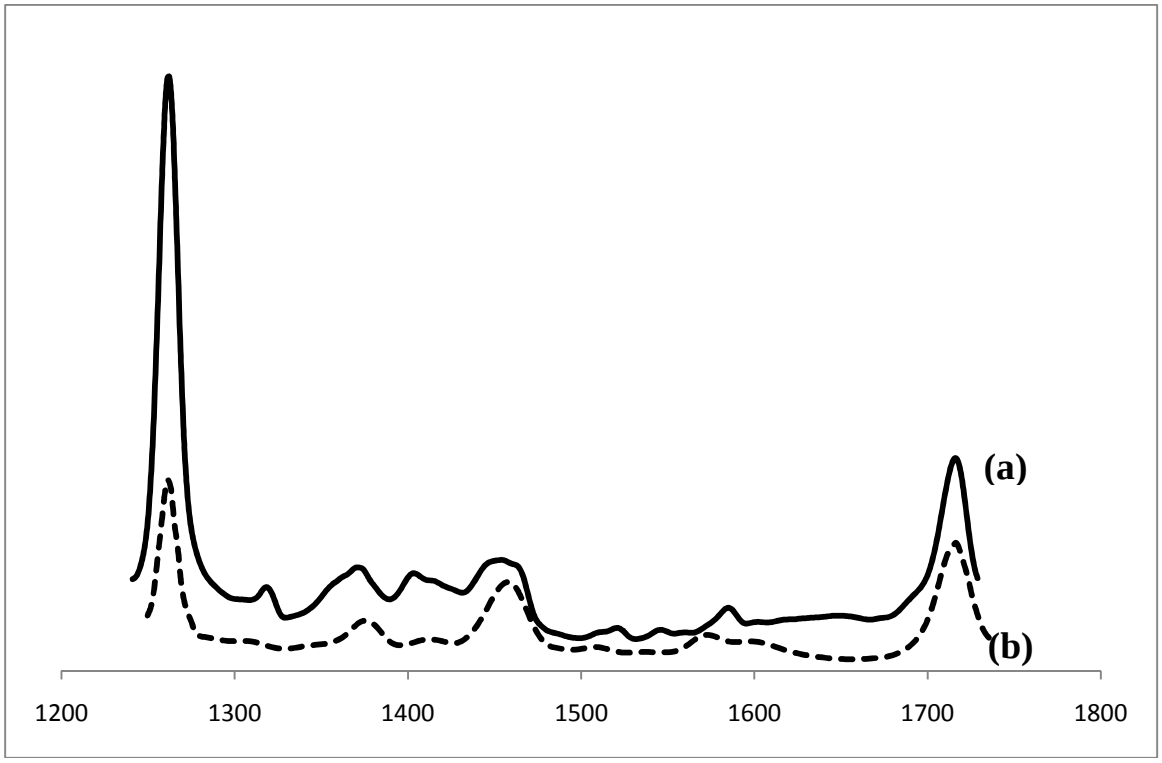

Figure 3-7. IR spectrum of (a) H_2OEPone (solid line) and the deuteration product (b) H_2OEPone-d_{12} (dash line) in KBr matrix

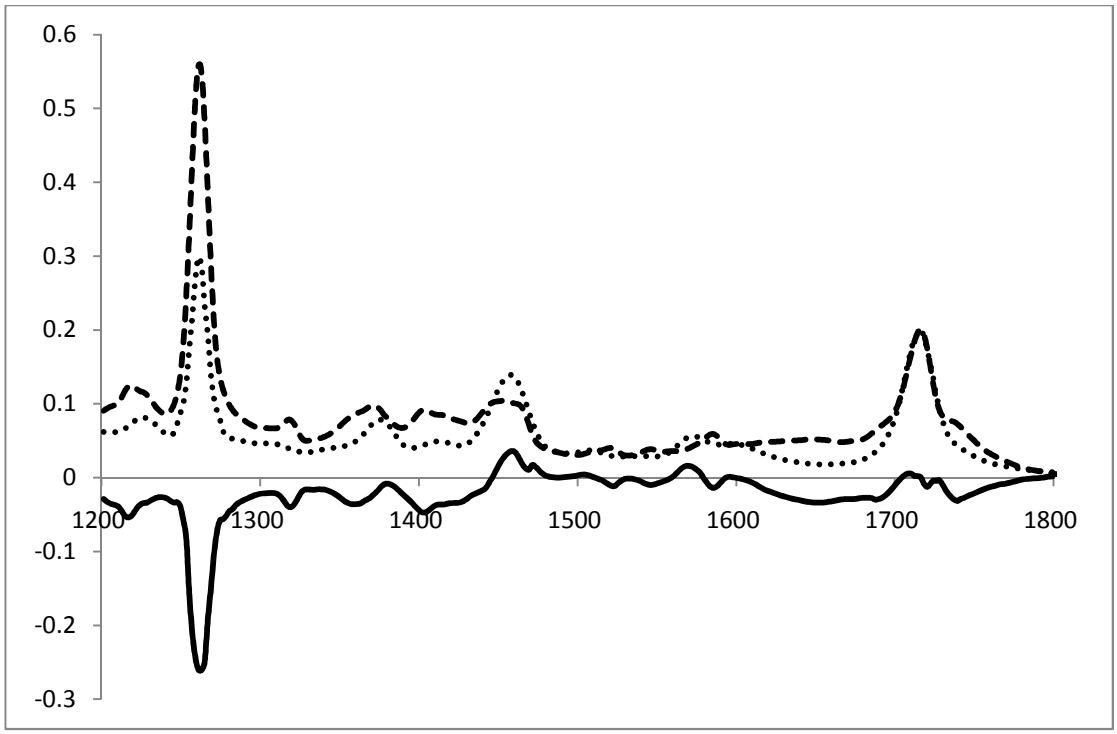

(a)

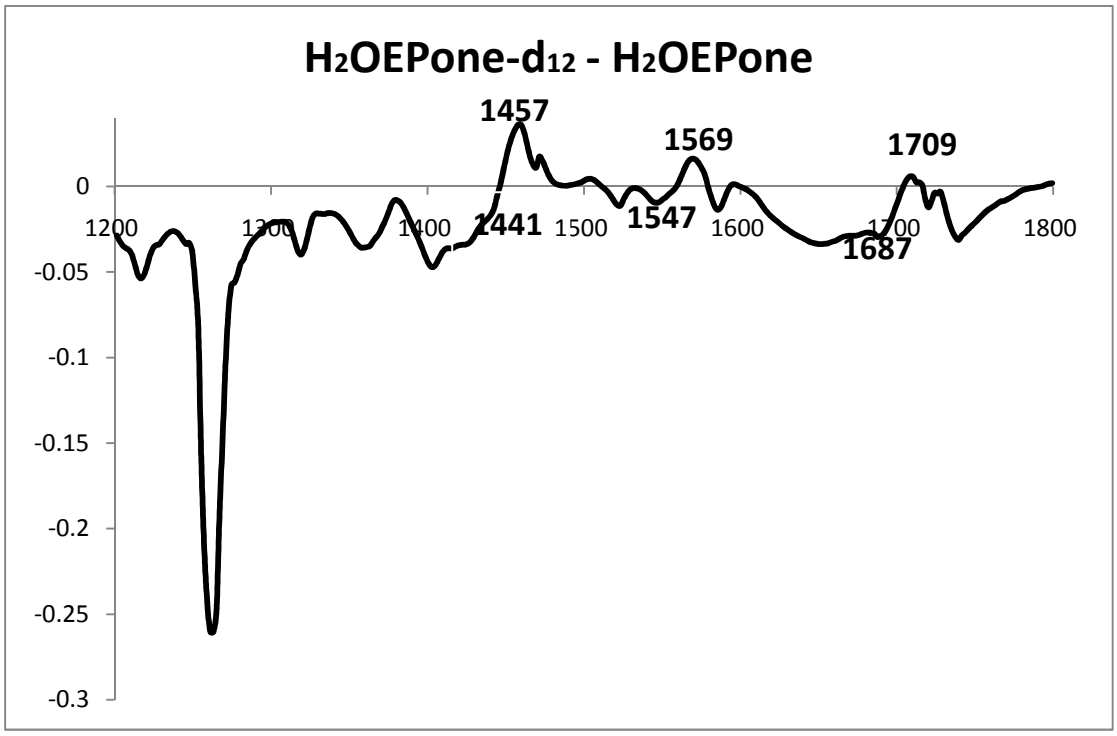

(b)

Figure 3-8. IR spectrum of (a) H_2OEPone, its deuteration product and the difference: Dash line(H_2OEPone); Dot line (H_2OEPone-d_{12}); Solid line (H_2OEPone-d_{12}−H_2OEPone) (b) the difference between H_2OEPone and H_2OEPone-d_{12} (H_2OEPone-d_{12} - H_2OEPone)

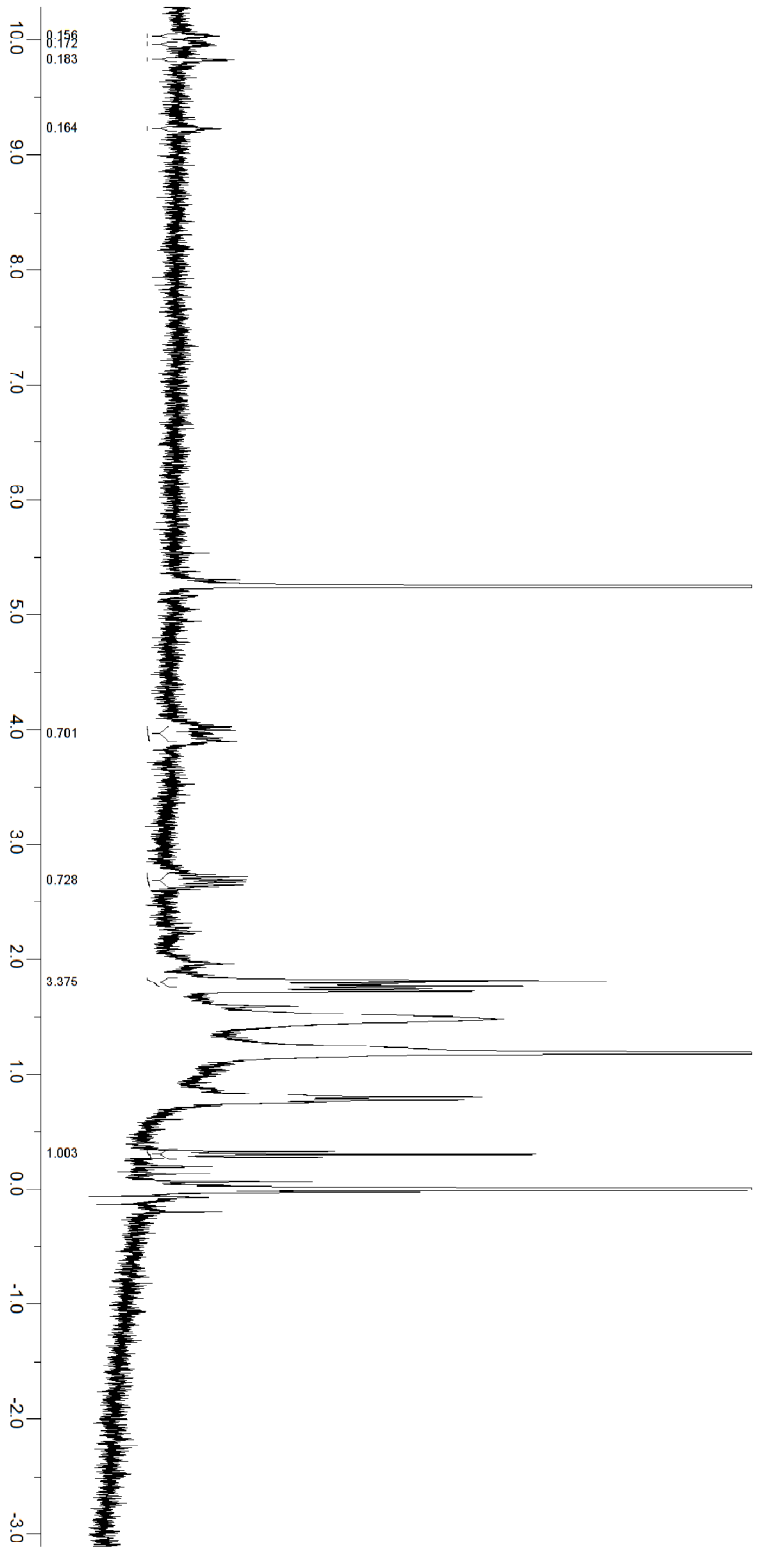

Figure 3-9. Proton NMR spectrum of the deuterated product H_2(OEPone)-d_{12} in CD_2Cl_2

3-3. UV-visible, infrared and Raman spectrum of the two electron reduced iron(III) tetraphenylporphyrin complex

The UV-visible absorption spectrum of the reduction product $[FeTPP]^-$ are shown in Figure 3-10. It is consistent with the work done by Reed et al[32], which showed that the λ_{max} (wavelengh/nm) are 426, 506, 572 and 612. Due to the high concentration, the Soret band of $[FeTPP]^-$ is off scale. The bands (wavelengh/nm) at 358 and 378 are due to anthracene.

The UV-visible spectrum of the reduction product $[FeTPP]^-$ and the starting material $Fe^{III}TPPCl$ are shown in Figure 3-11. There is a successive red shift of the Soret band (wavelengh/nm) from 414 to 426 during the reduction from $Fe^{III}TPPCl$. It reflects the extent of stabilization of the porphyrin π system after the reduction.

The UV-visible spectra of $Fe^{II}(TPP)$, $[Fe(TPP)]^-$ and $[Fe(TPP)]^{2-}$ in the THF solution were previously obtained by Reed[13] et al. The $Fe^{II}TPP$ (high spin, HS) has λ_{max} (wavelengh/nm) values of 426 (Soret), 539, 610 and $[Fe(TPP)]^{2-}$ has λ_{max} (wavelength/nm) at 572 and 618, while the λ_{max} (wavelength/nm) of $[Fe(TPP)]^-$ are 426, 510, 572 and 608. Thus, the reduction product we have obtained is most close to the low spin $[FeTPP]^-$ based on the absorption spectrum.

In Figure 3-12, the infrared spectra of $Fe^{III}TPPCl$ and the reduction product

[Fe(TPP)]$^{-}$ were obtained in KBr matrix. The infrared spectra data are summarized in Table 3-3 below.

Table 3-3. The infrared spectrum of iron tetraphenylporphyrin complexes

infrared spectrum (cm^{-1})	
$Fe^{III}TPPCl$	$[FeTPP]^{-}$
1030	
1069	1069
1159	1156
1174	1177
1201	1201
	1227
1277	1261
1298	1297
1335	1337
1364	1366
1388	
1440	1441
1485	1487
1505	
1527	1526
1547	1551
1570	1575
1596	1597

From Table 3-3, we find several bands (υ, cm^{-1}) move to lower frequencies after the reduction, which are 1159 to 1156, 1298 to 1297, 1527 to 1526 and 1277 to 1261 cm^{-1}. The band at 1277 cm^{-1} moved to 1261 cm^{-1} which is a dramatic downshift by 14 cm^{-1}. Some bands (υ, cm^{-1}) move to higher frequencies after the reduction, which are 1174 to 1177, 1335 to 1337, 1364 to 1366, 1440 to 1441, 1485 to 1487, 1547 to 1551, 1570 to 1575 and 1596 to 1597 cm^{-1}. The strong vibrational band at 1174 cm^{-1} for Fe^{III}(TPP)Cl not only upshifted by 3 cm^{-1}, but also became much weaker after the reduction which is a big change. The new band at 1227 is produced, while bands (υ, cm^{-1}) at 1030, 1388 and 1505 disappear after the reduction.

The resonance Raman spectrum shown in Figure 3-13 was measured with 1.0-0.9 mW in KBr powder to avoid the decomposition of the products. It was also measured with higher power (5.0 mW) and the increased power did not cause any changes. For convenience, we retain the nomenclature traditionally used for octaalkylporphyrins and refer to these modes as ν_4 and ν_2[15]. The Raman spectrum data are summarized in Table 3-4 below.

From Table 3-4, we can see that the ν_4 mode of $[FeTPP]^-$ is at 1361 cm^{-1}, which is 5 cm^{-1} higher than that of low spin $[FeTPP]^-$ reported by Bocian. The ν_2 mode is 3 cm^{-1} lower, which is 1552 cm^{-1} versus 1555 cm^{-1}. The ν_4 mode (cm^{-1}) of $[FeTPP]^-$ in this work differ 17 cm^{-1}, 7 cm^{-1} and 9 cm^{-1} respectively from high spin[15], low spin[15] and intermediate spin[62] of Fe^{II}TPP. The ν_2 mode (cm^{-1}) of $[FeTPP]^-$ in this work differ 12 cm^{-1}, 7 cm^{-1} and 13 cm^{-1} respectively from high spin[15], low spin[15] and intermediate spin[62] of

$Fe^{II}TPP$. However, we found there are 1076 cm^{-1} and 1236 cm^{-1} which are due to Fe(II) species.

While the UV-visible spectra of $[FeTTP]^-$ is consistent with what was obtained by Reed[32]. Because of the low Raman scattering of $[FeTTP]^-$, small amount of FeTPP will dominate the spectrum. Unfortunately, the 457.9 nm excitation which was used by Bocian for $[FeTTP]^-$ was not available at this time. As a result, it was difficult to separate the weak iron(I) bands from the strong iron(II) bands.

Table 3-4. The resonance Raman spectrum of the iron tetraphenylporphyrin complexes

	ν_4 (cm^{-1})	ν_2 (cm^{-1})	Other (cm^{-1})	Reference
FeTPP (high spin, in DMF, λ_{ex} = 413.1 nm)	1344	1540	1074, 1232	14
FeTPP (low spin in DMF, λ_{ex} = 413.1 nm)	1354	1559	1073, 1228	14
FeTPP(intermediate spin, in CH_2Cl_2, λ_{ex} = 457.9 nm)	1370	1565	1082, 1240	62
$[FeTPP]^-$ (low spin, in DMF, λ_{ex} = 457.9 nm)	1356	1555	1060, 1224	14
$[FeTPP]^-$ (in KBr solid matrix, λ_{ex} = 413.1 nm)	***1361***	***1552***	1076, 1236	this work

Based on the absorption spectrum we have obtained, we found that the results matched that from Reed[13]. Meanwhile, from infrared spectra, we have a downshift of several bands, indicating an increase of the electron density on the macrocyclic ring.

There has been little analysis of the infrared spectra of FeTPP and its reduced product. It is difficult to compare our results with the predicted shifts at this time.

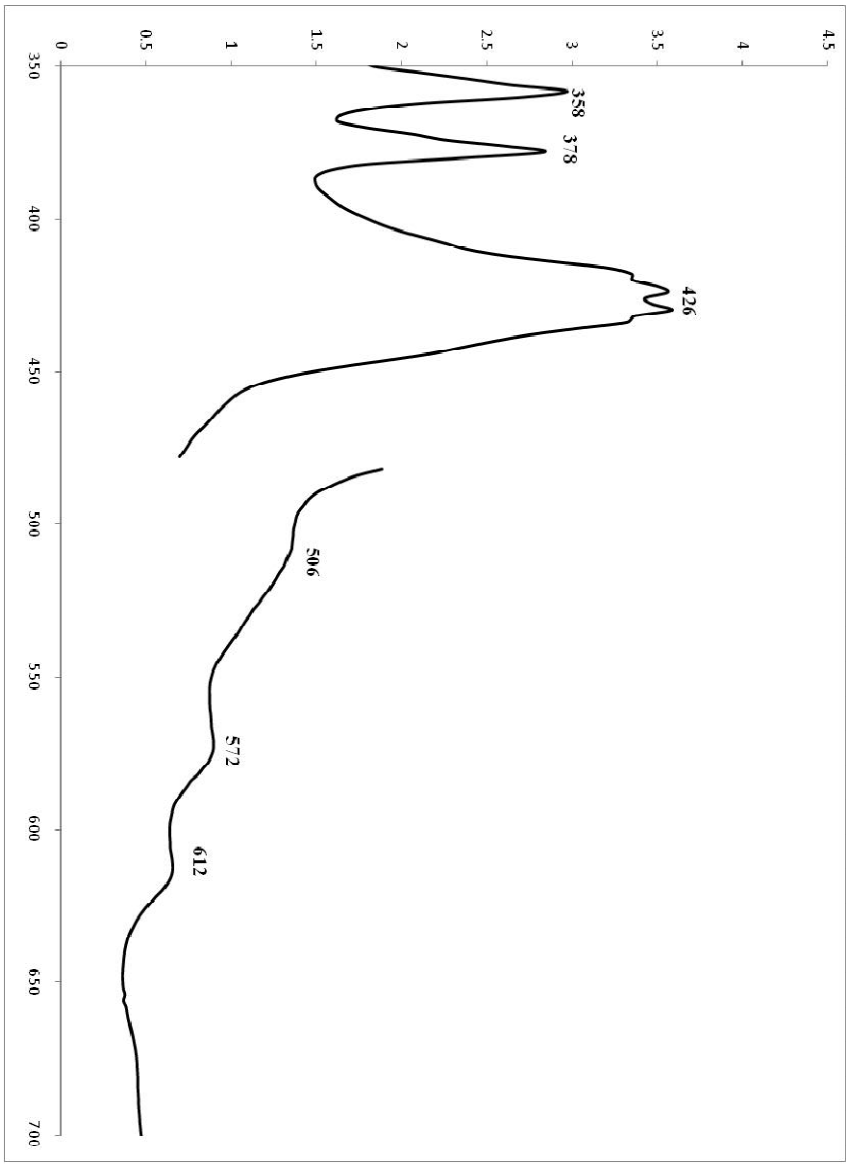

Figure 3-10. UV-visible of the reduction product $[FeTPP]^-$ in THF solution

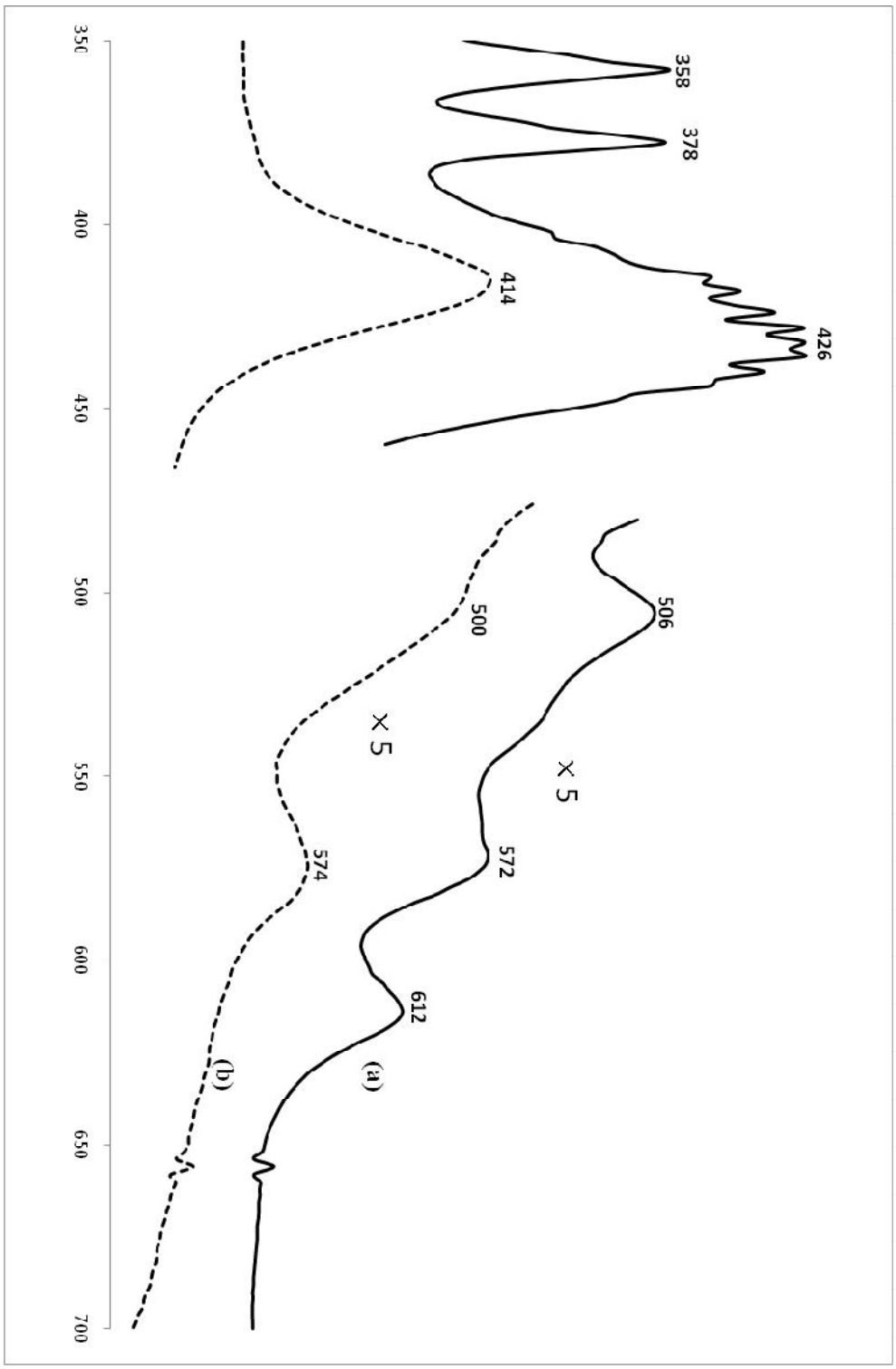

Figure 3-11. UV-visible of (a) $[FeTPP]^-$ (solid line) and (b) $Fe^{III}TPPCl$ (dash line) in THF solution

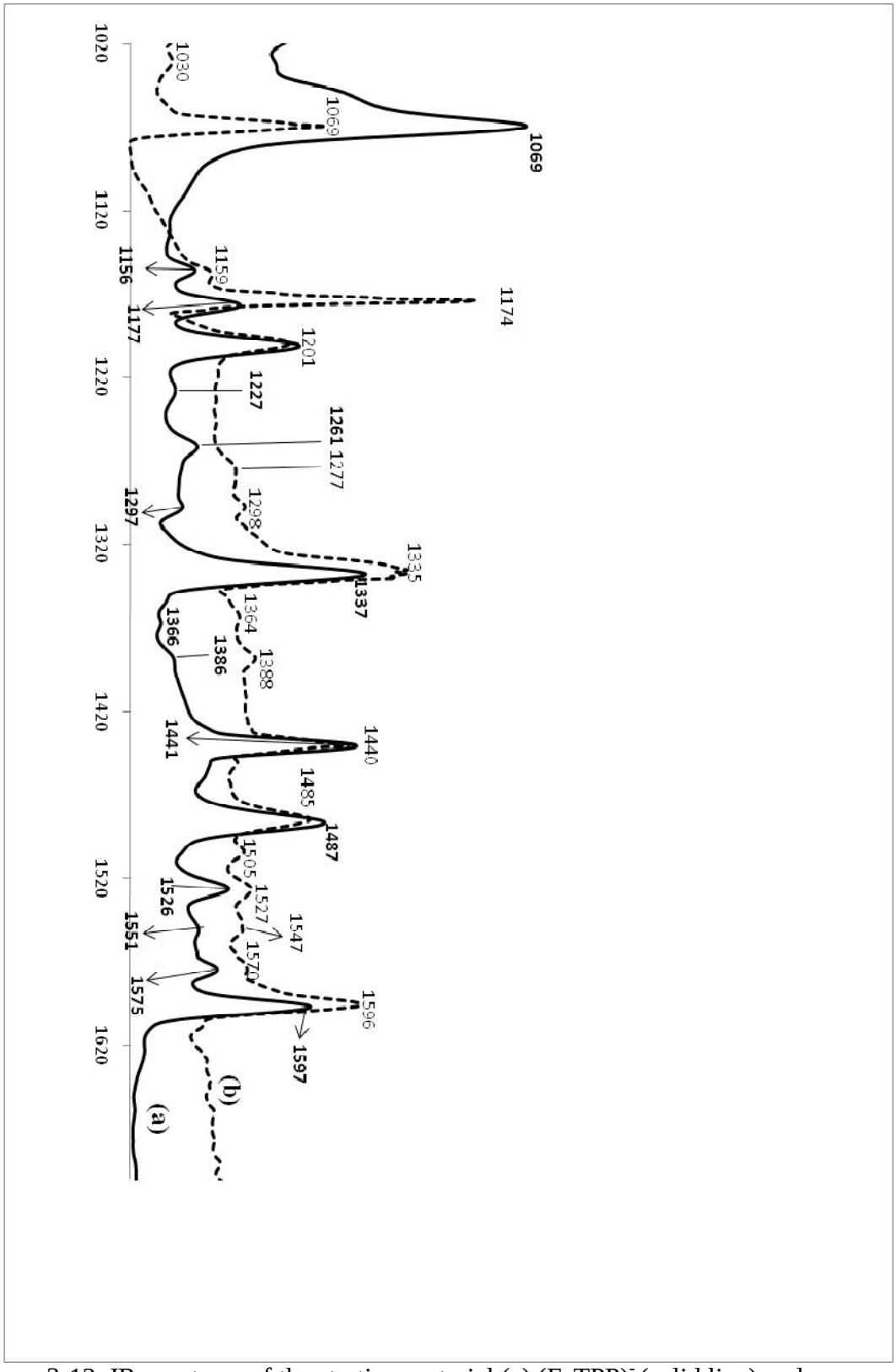

Figure 3-12. IR spectrum of the starting material (a) $(FeTPP)^{-}$ (solid line) and (b) $Fe^{III}TPPCl$ (dash line) in KBr matrix

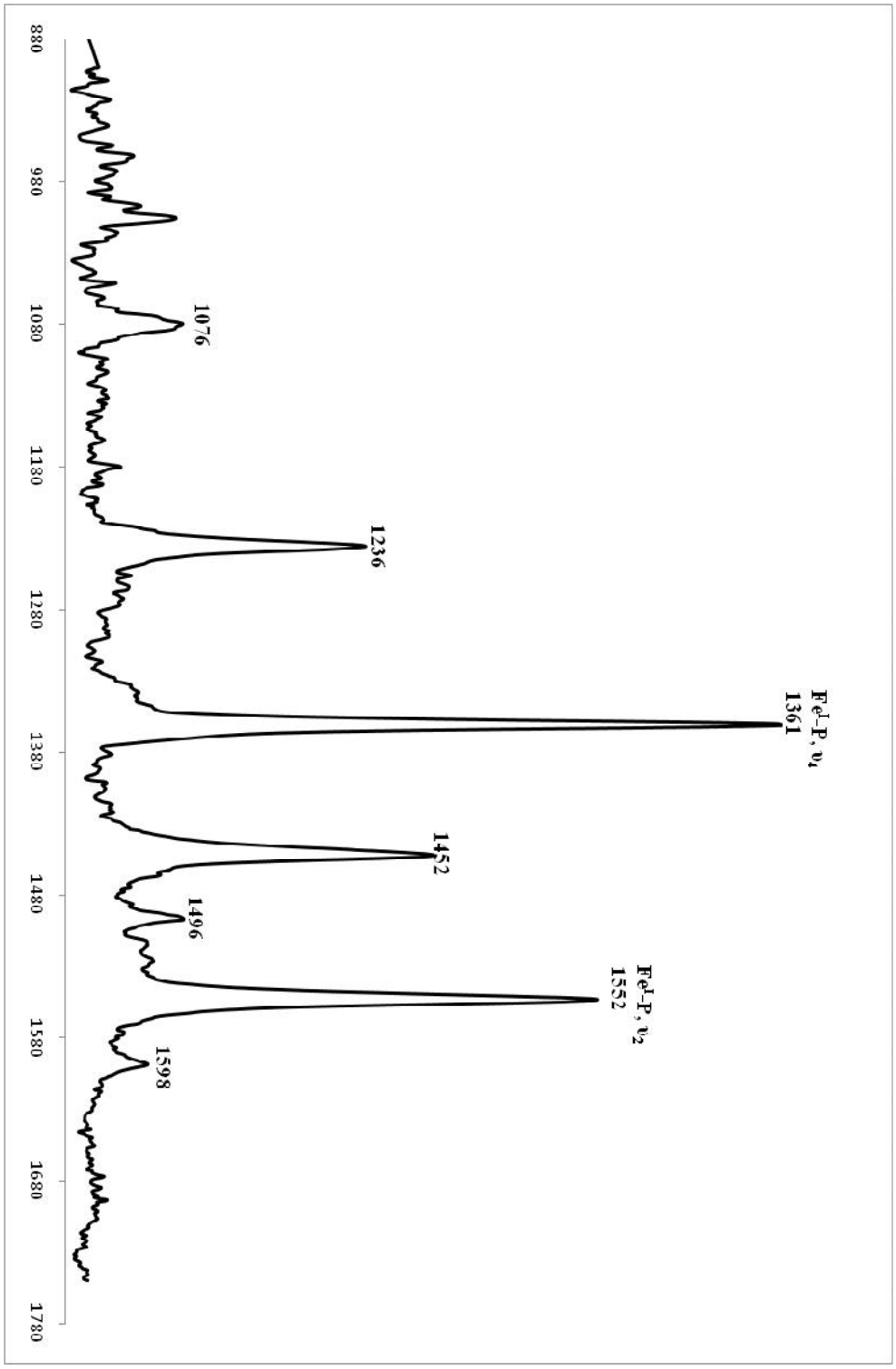

Figure 3-13. The resonance Raman spectrum of iron tetraphenylporphyrin complexes measured with 1.0-0.9 mW in KBr powder (λ_{ex} = 413.1 nm)

3-4. UV-visible, infrared and Raman spectrum of the two electron reduced iron(III) octaethylporphyrin complex

The UV-visible of the starting material $Fe^{III}OEPCl$ and the reduction product $[FeOEP]^-$ are shown in Figure 3-14. To better analyze the product that we obtained, we compared our absorption peaks with what have been done by Teraoka[39] in Table 3-5. The reduction process can be written as:

$Fe^{III}OEPCl$ + Sodium anthracenide →

$$[Fe(OEP)]^- + Cl^- + \text{anthracene} + Na^+$$

Table 3-5. The UV-visible spectrum of iron octaethylporphyrin complexes

Compounds	B bands (nm)	Q bands (nm)	References
$Fe^{II}(OEP)(THF)$	407	558	39
$(FeOEP)^{2-}$	356, 440	N/A	39
$Fe^{III}OEPCl$	372, 400	508, 532,630	this work
$(Fe^{I}OEP)^-$	373, 419, 455	N/A	39
$[FeOEP]^-$	373, 407, 414, 454	516, 558, 664	this work

From Table 3-5, the Soret region of the reduction product $[Fe(OEP)]^-$ is affected by another product of the reduction reaction, anthracene, and also the possible byproduct $Fe^{II}(OEP)(THF)$[39]. The bands of anthracene overlap the iron(I) complex making the

Soret bands different from that obtained byTeraoka[39] . But it is clear that the Soret bands (wavelength/nm) become broader and have a red shift after the reduction. Our reduced product has the absorption peaks (wavelength/nm) at 419 and 454 which are close to that of $(Fe^{I}OEP)^{-}$ by Teraoka[39]. However, the absorption peaks (wavelength/nm) at 407 and 558 are close to $Fe^{II}(OEP)(THF)$ by Teraoka[39]. Thus, our reduced product is close to $(Fe^{I}TPP)^{-}$ with some impurity $Fe^{II}(OEP)(THF)$ inside based on the UV-visible spectrum.

The IR spectra of the starting material $Fe^{III}OEPCl$ and the reduction product $[FeOEP]^{-}$ are given in Figure 3-15. The bands are summarized in Table 3-6 below.

From Table 3-6, we find that new bands (υ, cm^{-1}) at 1196, 1248 and 1587 appear but bands (υ, cm^{-1}) at 1122 and 1358 disappear after reduction from $Fe^{III}OEPCl$. For the bands at the same wavenumbers, the strength of the absorption is quite different. For example, the absorption bands (υ, cm^{-1}) at 1146, 1268 and 1313 become much weaker after reduction. The difference during the reduction of infrared spectrum indicates the possibilities of reduction. There has been little analysis of the infrared bands of the reduced product $[FeOEP]^{-}$ in KBr matrix. It is difficult to compare our result with the predicted shifts at this time.

Table 3-6. The infrared spectra of iron octaethylporphyrin complexes

Vibration bands (υ, cm^{-1})	
$Fe^{III}OEPCl$	$[FeOEP]^-$
1109	1109
1122	
1146	1146
	1196
1213	1213
1252	1248
1268	1268
1313	1313
1358	
1371	1371
1468	
1494	
	1587

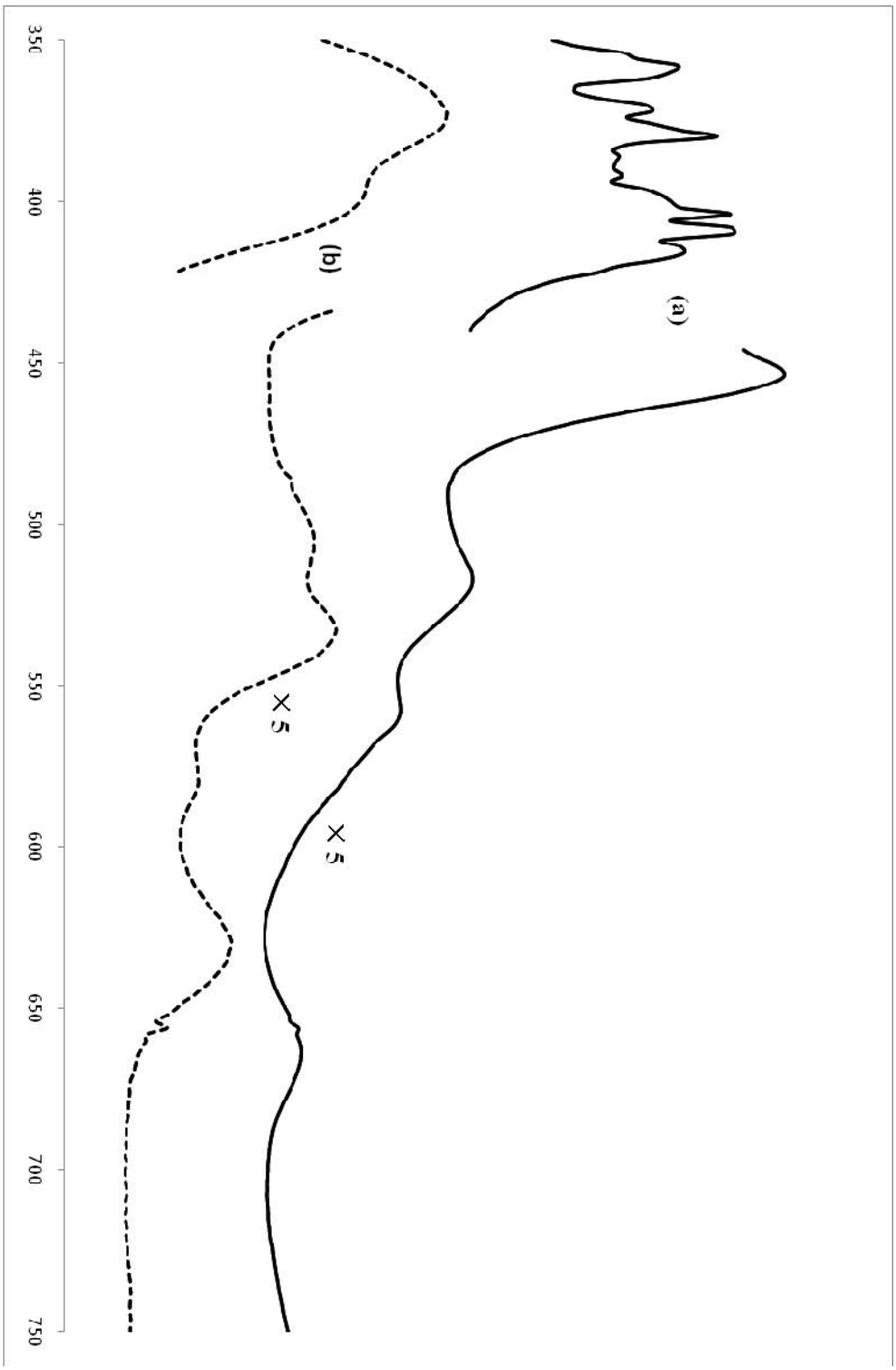

Figure 3-14. UV-visible spectrum of (a) $(FeOEP)^-$ (solid line) and (b) $Fe^{III}OEPCl$ (dash line) in THF solution.

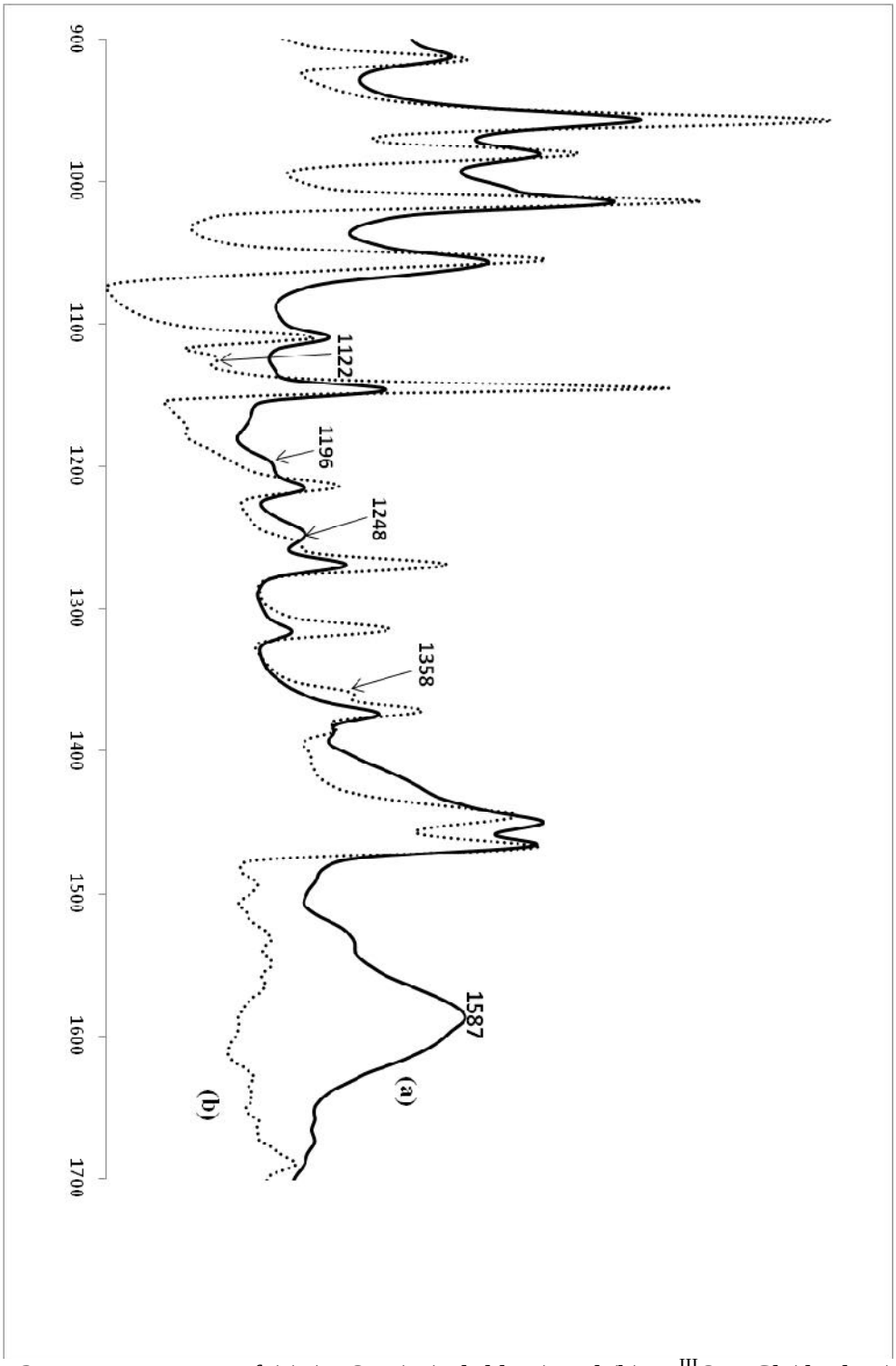

Figure 3-15. IR spectrum of (a) $(FeOEP)^-$ (solid line) and (b) $Fe^{III}OEPCl$ (dot line) in KBr matrix.

3-5. UV-visible and infrared spectrum of iron(III) porphinone chloride

The UV-visible spectrum of H_2OEPone and Fe^{III}(OEPone)Cl are shown in Figure 3-16. The absorption spectrum of Fe^{III}(OEPone)Cl are consistent with the result by Wei[38], which shows that the insertion of '-Fe^{III}Cl' is successful. For better comparing the starting material H_2OEPone and the product Fe^{III}(OEPone)Cl, the absorption data are summarized in Table 3-7 below.

Table 3-7. The absorption spectra of iron porphinone and free base porphinone complexes

Compounds (Solution)	B bands (nm)	Q Bands (nm)	Reference
H_2OEPone (THF)	406	506, 548, 582, 642	this work
Fe^{III}(OEPone)Cl (THF)	386, 486	514, 556, 600, 658	this work
Fe^{III}(OEPone)Cl (CH_2Cl_2)	384 (11.50 $mM^{-1}cm^{-1}$), 486 (1.581)	517(1.40), 551(1.205), 599(2.19), 661(0.436)	53
Fe^{III}(OEPone)Cl (THF)	386 (66 $mM^{-1}cm^{-1}$), 482 (8.3)	546(6.6), 596(14), 658(3.5), 730(3.6)	37

From Table 3-7, we can see the spectrum of the product Fe^{III}(OEPone)Cl are consistent with that obtained by Cai[53] and Liu[37]. Comparing the UV-visible spectrum of the starting material H_2OEPone with the product Fe^{III}(OEPone)Cl we obtained, the Soret band blue shifts from 406 nm to 386 nm and becomes broadened which showed that the π

system of the porphinone has been destabilized after the insertion of '-$Fe^{III}Cl$' .

The FT-IR spectrum of H_2OEPone and Fe^{III}OEPoneCl are shown in Figure 3-17 and Figure 3-18. The vibrations are summarized in the Table 3-8 below:

Table 3-8: The infrared spectroscopy of free-base and iron porphinone complexes in KBr

compound	υ_{CO} (cm^{-1})	Other bands (cm^{-1})	References
H_2OEPone	1716	1585, 1544, 1520, 1454, 1402, 1371, 1318, 1262, 1218, 1184, 1096, 1054, 1011	this work
Fe^{III}(OEPone)Cl	1713	1666, ***1562, 1535***, 1490, 1454, ***1389***, 1318, ***1271, 1225***, ***1208***, 1144, 1119, 1056, 1011	this work
Fe^{III}(OEPone)Cl	1719	***1563, 1536, 1383, 1268, 1228,*** 1221, ***1209,*** 754, 732	38

From Table 3-8, we can see the Fe^{III}OEPoneCl we obtained have many bands with the same or similar wavenumbers as that by Wei[38]. The υ_{CO} band is 1713 cm^{-1}, which is 6 cm^{-1} lower than that by Wei. For other bands, the similar peaks are highlighted in Table 3-8 which shows that our product is quite close to the Fe^{III}(OEPone)Cl by Wei.

From Table 3-8, we find that when the iron inserted into the free base H_2OEPone, the υ_{CO} position doesn't change significantly (1716 cm^{-1} to 1713cm^{-1}). For the typical infrared absorption frequencies, the stretching vibration of C-N is between 1000 and 1250cm^{-1}

and the bending vibration of NH_2 scissoring is between 1550 cm^{-1} to 1650 cm^{-1}. We emphasized the IR spectra between 1000 cm^{-1} and 1250 cm^{-1} in Figure 3-19 (a) and 1550 cm^{-1} to 1650 cm^{-1} in Figure 3-19 (b). From Figure 3-19, we can see the vibrations at 1184 cm^{-1} and 1093 cm^{-1} disappeared; the band at 1585 cm^{-1} downshifted to 1562 cm^{-1} and the number of the vibration bands became less after the metal insertion.

These vibrational changes probably were due to the electron density had been changed dramatically. And the symmetry of the molecule increased which simplified the vibration species after the iron(III)Cl exchanging two protons in NH positions.

In a word, the insertion of '-Fe^{III}Cl' to free base porphinone is successful. The structure of Fe^{III}(OEPone)Cl from Scheidt is shown in Figure 3-20[35]. The success of the reduction can be approved by both UV-visible spectrum and infrared spectrum. The product is the desired Fe^{III}OEPoneCl by comparing the infrared spectrum with what was observed by Wei[38].

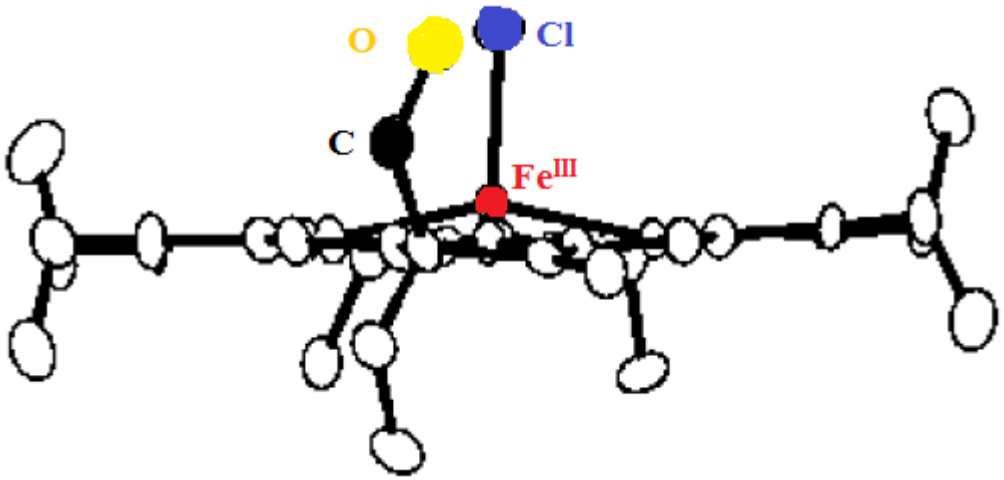

Figure 3-20. The structure of Fe^{III}OEPoneCl[35]

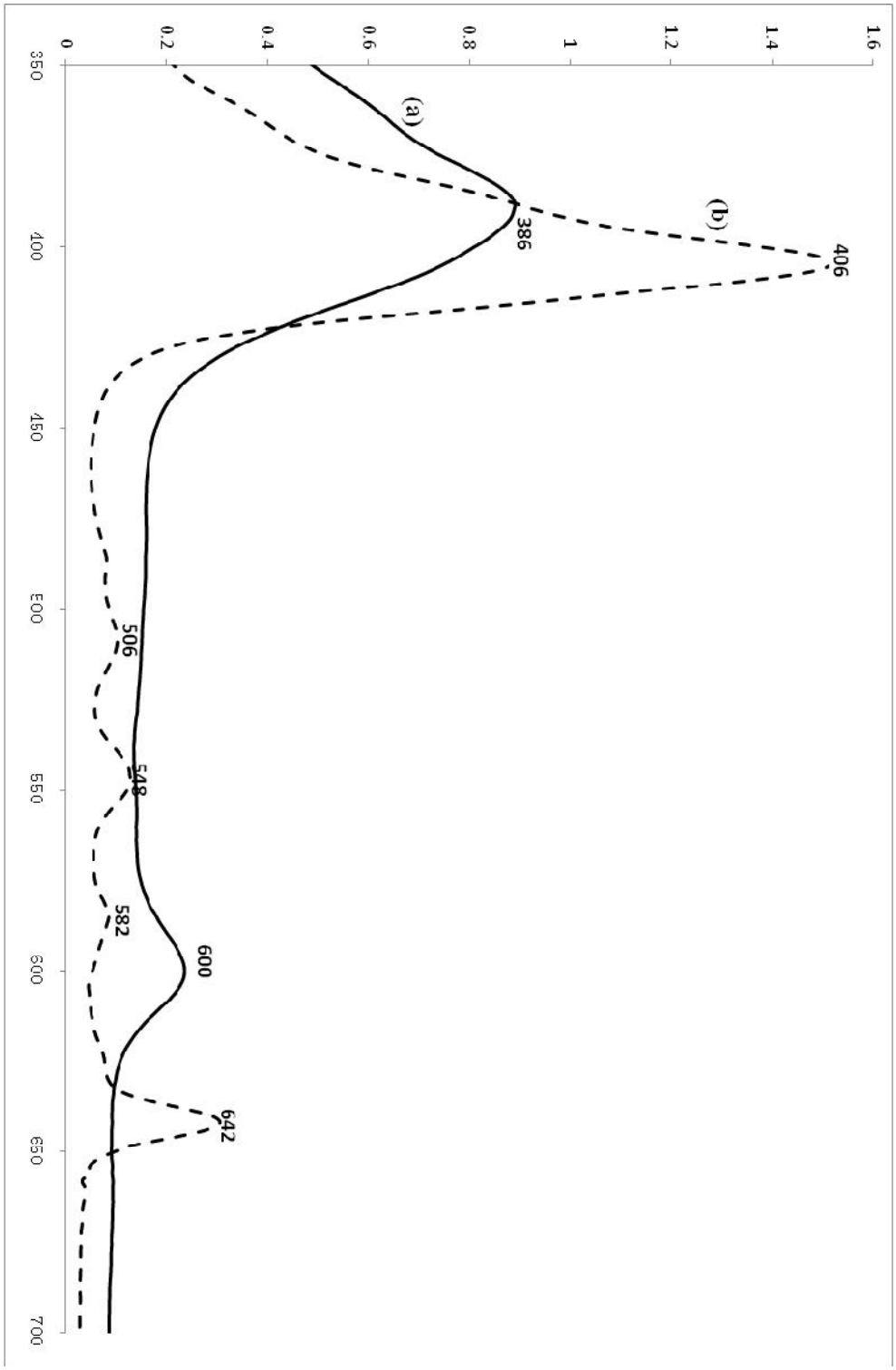

Figure 3-16. UV-visible spectrum of (a) Fe^{III}OEPoneCl (solid line) and (b) H_2OEPone (dash line)

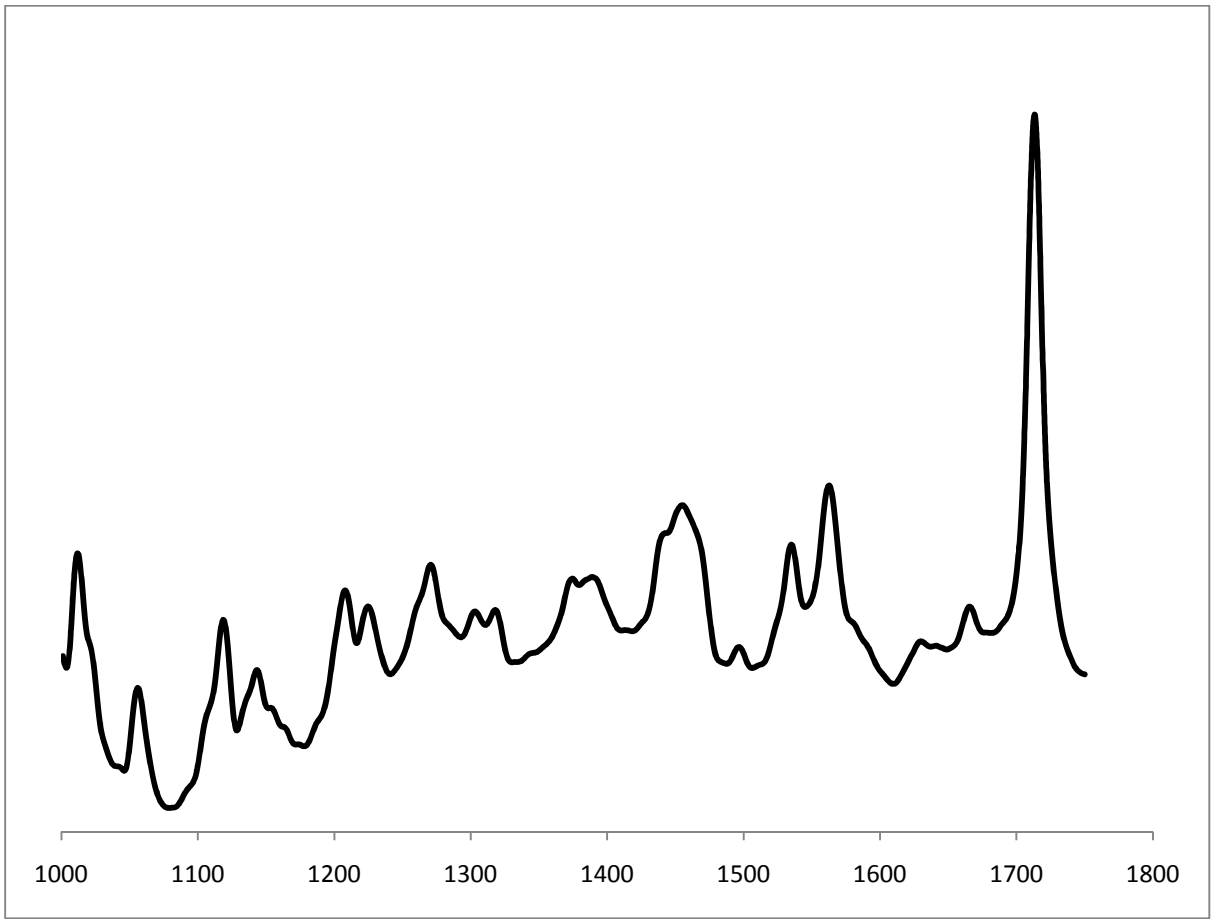

Figure 3-17. IR spectrum of Fe^{III}(OEPone)Cl in KBr matrix

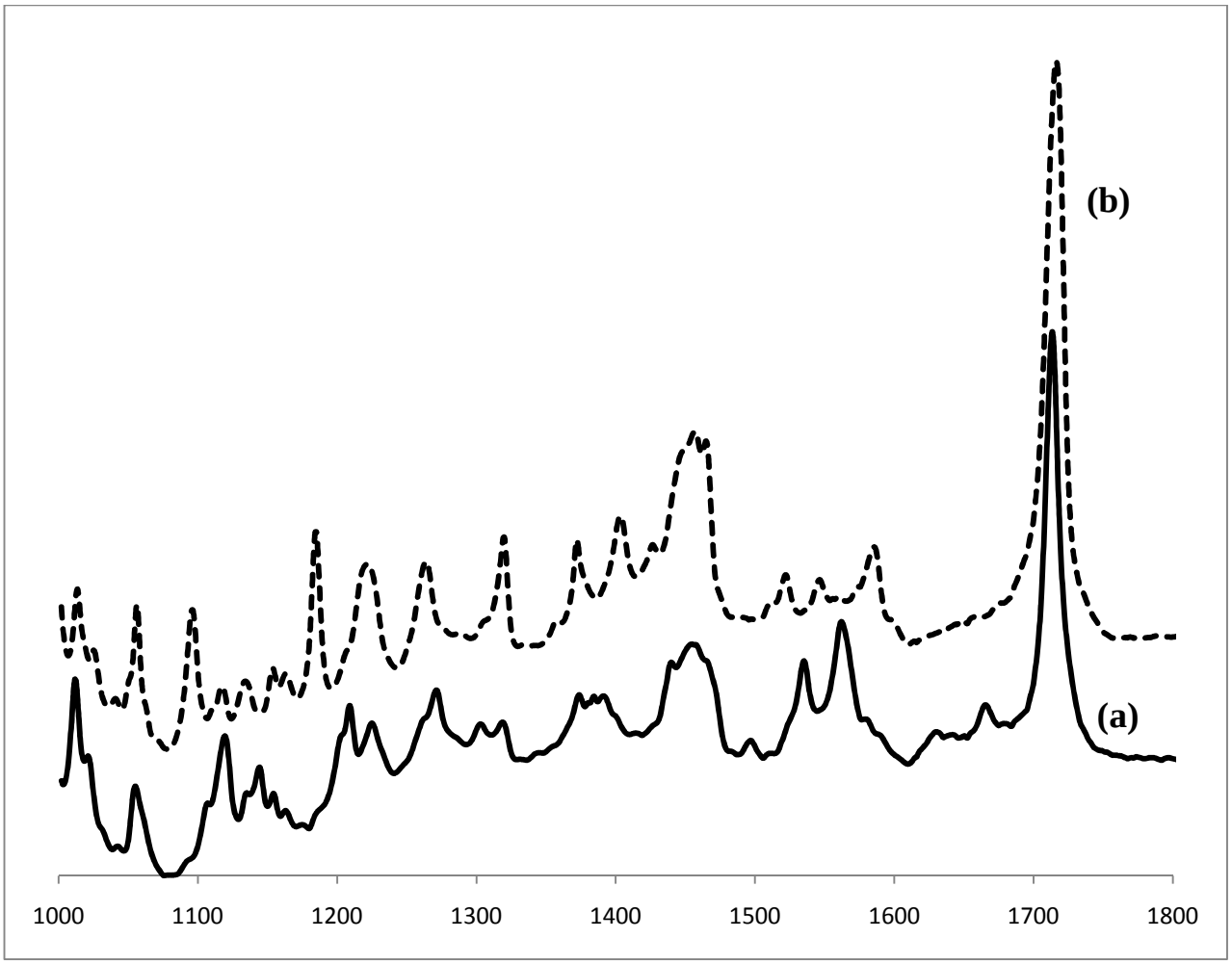

Figure 3-18. Infrared spectrum of the free base porphinone and iron porphinone complexes in KBr powder: (a) FeOEPoneCl (solid line); (b) H_2OEPoneCl (dash line)

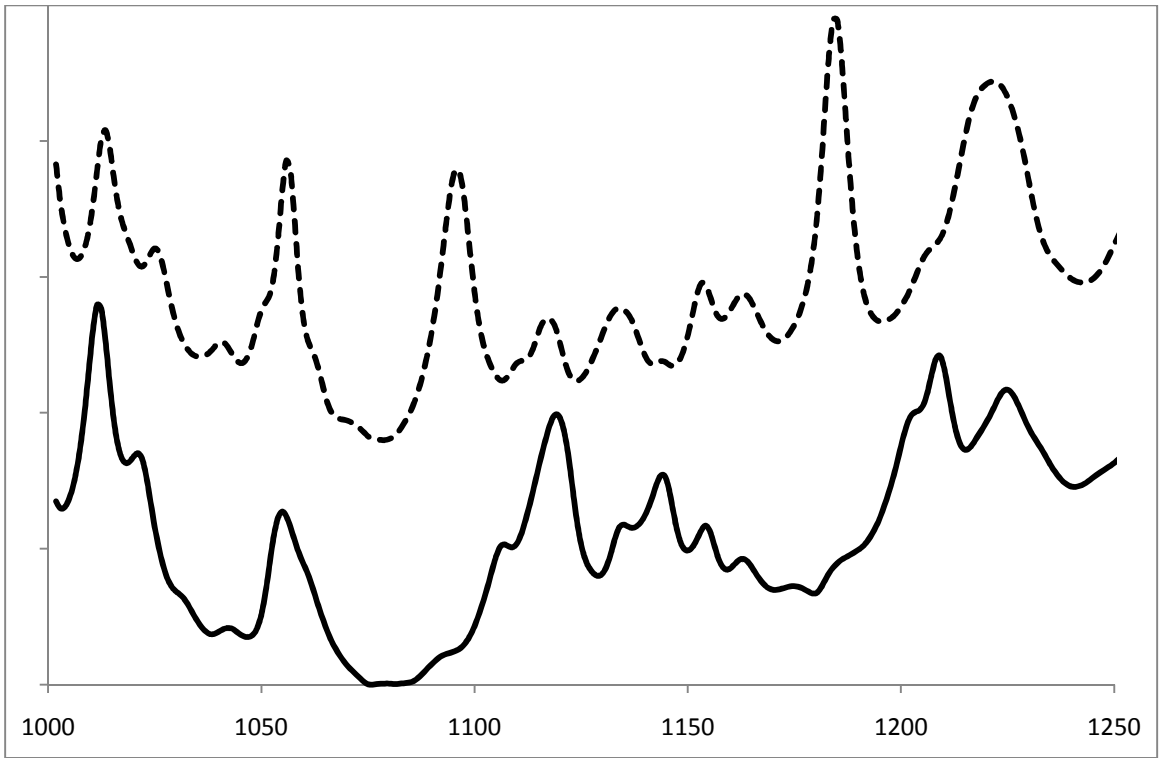

(a)

(b)

Figure 3-19. Infrared spectrum of free base porphinone and iron porphinone complexes in KBr powder: (a) 1000 cm^{-1} – 1250 cm^{-1}; (b) 1550 cm^{-1} -1650 cm^{-1}.

3-6.UV-visible, infrared and Raman spectrum of the two electron reduced iron(III) porphinone complex

The UV-visible spectrum of Fe^{III}OEPoneCl and its reduced product, $[Fe(OEPone)]^-$, are shown in Figure 3-21. The absorption spectrum was compared to that obtained by Liu[37] who did the reduction in OTTLE spectroelectrochemistry. The UV-visible spectra were summarized in Table 3-9. The reaction for the reduction process is:

$Fe^{III}OEPoneCl$ + Sodium anthracenide →

$[Fe(OEPone)]^-$ + Cl^- + anthracene + Na^+

Table 3-9. UV-visible spectrum of iron porphinone complexes in THF solution

	B bands (nm)	Q bands (nm)	Reference
Fe^{III}(OEPone)Cl	386 , 482	546 , 596, 658 , 730	37
Fe^{III}(OEPone)Cl	386 , 486	514 , 556 , 600 , 658	this work
$[Fe(OEPone)]^-$	364, 407, 446	522 , 585 , 645	37
$[Fe(OEPone)]^-$	358, 378, 394	526 , 538, 572 , 584, 650	this work
Fe^{II}(OEPone)	399, 413, 486	545, 594 , 661	37

From Table 3-9, the Soret region of the reduction product $[Fe(OEPone)]^-$ is affected by another product of the reduction reaction, anthracene. The bands of anthracene overlap the rion(I) complex making the Soret bands different from that obtained by Liu[37] . But it is clear that the Q band at 596 nm for both Fe^{III}OEPoneCl and Fe^{II}OEP have

completely disappeared, and the new band at 650 nm appears, indicating the complete reduction to the iron(I) complex.

The infrared spectrum of the reduced product $[Fe(OEPone)]^-$ are shown in Figure 3-22. Figure 3-23 gives the infrared spectrum of both the starting material $Fe^{III}OEPoneCl$ and the reduced product $[Fe(OEPone)]^-$. Wei examined the infrared spectroelectrochemical reduction of iron porphinone complexes using spectroelectrochemistry. To comparing the infrared spectrum with that obtained by Wei, the infrared spectrum data are summarized in 3-10 below.

Table 3-10. The infrared spectrum of iron porphinone complexes

compound	υ_{CO} (cm^{-1})	Other bands (cm^{-1})	Reference
Fe^{III}(OEPone)Cl	1713	1666, 1562, 1535, 1454, 1389, 1318, 1271, 1225, 1208, 1144, 1119, 1056, 1011, 960, 916, 860	this work
Fe^{III}(OEPone)Cl	1719	1563, 1536, 1383, 1268, 1228, 1221, 1209, 754, 732	38
Fe^{II}(OEPone)	1703	1550, 1530, 1361, 1221, 754, 742	38
$[Fe^{I}OEPone]^-$	1663, 1580	1603, 1548, 1526, 1430, 1372, 1248, 982, 909	this work
$[Fe^{I}OEPone]$-	1671, 1578	1609, 1548, 1526, 1361, 1219, 728	38

From Table 3-10, we can see our reduction product has the υ_{CO} at 1663 and 1580 cm^{-1}, which are close to 1671 and 1578 cm^{-1} of $[Fe^{I}OEPone]^{-}$ by Wei[38]. The υ_{CO} downshifts over 50 cm^{-1} from 1713 cm^{-1} of $Fe^{III}(OEPone)Cl$ and splits to two peaks of 1663 and 1580 cm^{-1} which shows that the reduction are successful. The υ_{CO} downshifts from high energy to lower energy with over 50 cm^{-1} indicates a considerably weakening of the carbonyl group.

For other bands, there are many similarities. For example, the vibrations bands at 1548 cm^{-1} and 1526 cm^{-1} in the IR of our reduction products are also found in Wei's. And the 1603 cm^{-1} and 1372 cm^{-1} in the infrared spectrum of our reduced product is close to 1609 cm^{-1} and 1361 cm^{-1} by Wei. Thus, our reduced product is quite close to the desired $[FeOEPone]^{-}$ based on the infrared spectrum. Some differences may be due to the KBr matrix we use as opposed to the THF solution in Wei's work.

For the porphinone complex, the reduction is known to be metal centered. Although the reduction is primarily on the iron, some of the election density of the iron(I) d_{z^2} will delocalize to the porphinone macrocycle by back-bonding. Although iron(III) and iron(I) both have back-bonding to the porphinone, iron(I) has two more electrons than iron(III). There are more electrons to be used for back-bonding in iron(I) porphinone complex. Thus, the electron density on the macrocycle of $[Fe^{I}OEPone]^{-}$ is higher than that of $Fe^{III}OEPoneCl$, making the carbonyl group frequency decrease after the reduction.
The resonance Raman spectrum of $[Fe^{I}OEPone]^{-}$ samples shown in Figure 3-24 were measured at room temperature in KBr matrix. The excitation line was 406 nm and the

power on the sample was 1.0 – 0.9 mW, total collection time was three hours. The sample had very large background which led to considerable noise in the spectrum.

From Figure 3-24, the RR spectrum exhibits the frequencies at 1137, 1259, 1314, 1378, 1493, 1570, 1609 cm^{-1}. Since isotopically substituted [Fe^{I}OEPone]- haven't been done, it is difficult for us to assign the specific modes.

We know that if the vibration in the molecule changes the dipole moment, this molecular vibration is IR active; if the vibration changes the polarizability, the vibration is Raman active. And for some vibrations, they may be both IR and Raman active, thus can be seen both in IR and Raman spectrum. In Table 3-11 below, the IR and Raman spectrum of iron porphinone complexes will be compared in detail.

From Table 3-11, Raman spectra of the [Fe^{I}OEPone]$^{-}$ exhibited a vibration at 1671 cm^{-1} which is the same as the υ_{CO} of the IR by Wei[38]. There is a 1609 cm^{-1} band in our RR spectrum of [Fe^{I}OEPone]$^{-}$ which also can be found in the IR spectrum by Wei. Meanwhile, there are 1570, 1529, 1378 and 1363 cm^{-1} bands in the RR spectrum of [Fe^{I}OEPone]$^{-}$ which are close to 1578 (υ_{CO}), 1526, 1372 and 1361 cm^{-1} in the IR spectrum. What also should be noted is that the 1713 cm^{-1} (Fe^{III}OEPCl, υ_{CO}) and 1703 cm^{-1} (Fe^{II}OEP, υ_{CO}) could not be found in the Raman spectrum of [Fe^{I}OEPone]$^{-}$ indicating the high purity of our reduction product. Thus, from the comparison between the RR spectrum and IR spectrum, we may also conclude that the reduced product is the desired [Fe^{I}OEPone]$^{-}$ with few impurities of iron(II) or iron(III) porphinones.

Table 3-11. IR and Raman Comparison for iron porphinone complexes in KBr matrix

compound	Souce	Other bands (cm^{-1})	Ref.
Fe^{III}(OEPone)Cl	IR	1713 (υ_{CO}), 1666, 1562, 1535, 1454, 1389, 1318, 1271, 1225, 1208, 1144, 1119, 1056, 1011, 960, 916, 860	this work
Fe^{II}(OEPone)	IR	**1703 (υ_{CO})**, 1550, 1530, 1361, 1221, 754, 742	38
$[Fe^{I}OEPone]^-$	IR	**1671 (υ_{CO}), 1578 (υ_{CO})**, 1609, 1548, 1526, 1361, 1219, 728	38
$[Fe^{I}OEPone]^-$	IR	**1663 (υ_{CO}), 1580 (υ_{CO})**, 1603, 1548, 1526, 1430, 1372, 1248, 982, 909	this work
$[Fe^{I}OEPone]^-$	Raman	1671, 1609, 1570, 1529, 1493, 1378, 1363, 1314, 1259, 1137	this work

Based on the UV-visible spectrum, infrared spectrum and Raman spectrum we have obtained, we found that the reduction is successful and the reduced product is the desired $[Fe^{I}OEPone]^-$. During the comparison of the resonance Raman and infrared spectrum of $[Fe^{I}OEPone]^-$, we found many similarities in the bands, which shows that some peaks are both Raman and IR active. Since many IR vibrations of $[Fe^{I}OEPone]^-$ can be found in the Raman of $[Fe^{I}OEPone]^-$, but the C=O vibration of Fe^{II} or Fe^{III} porphinone complexes which are considerably strong peaks, the conclusion is that the reduction of Fe^{III}OEPoneCl is successful, the product is the desired $[Fe^{I}OEPone]^-$ with few impurities.

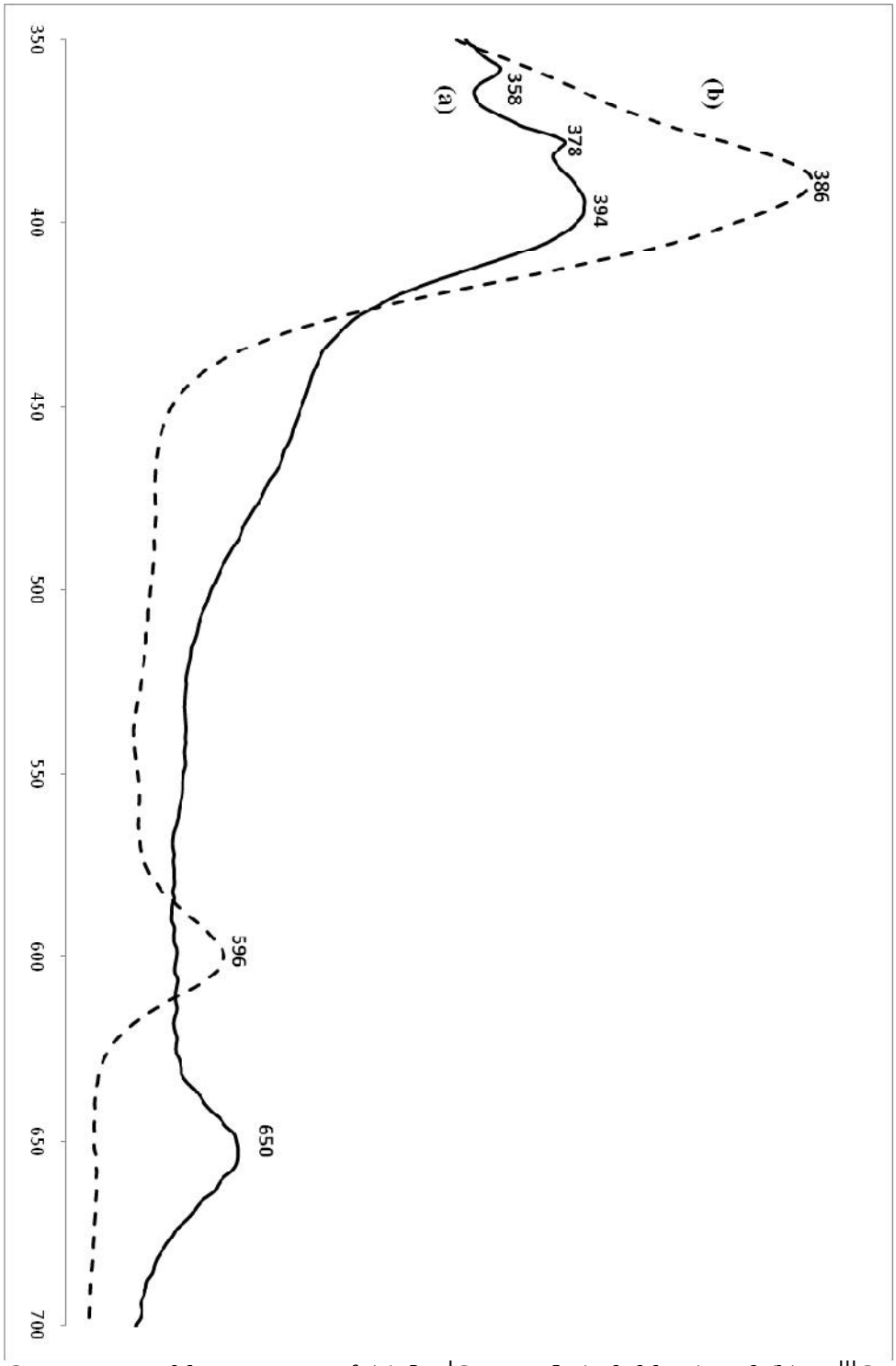

Figure 3-21. UV-visible spectrum of (a) $[Fe^{I}OEPone]^{-}$ (solid line) and (b) $Fe^{III}OEPoneCl$ (dash line) in THF solutions.

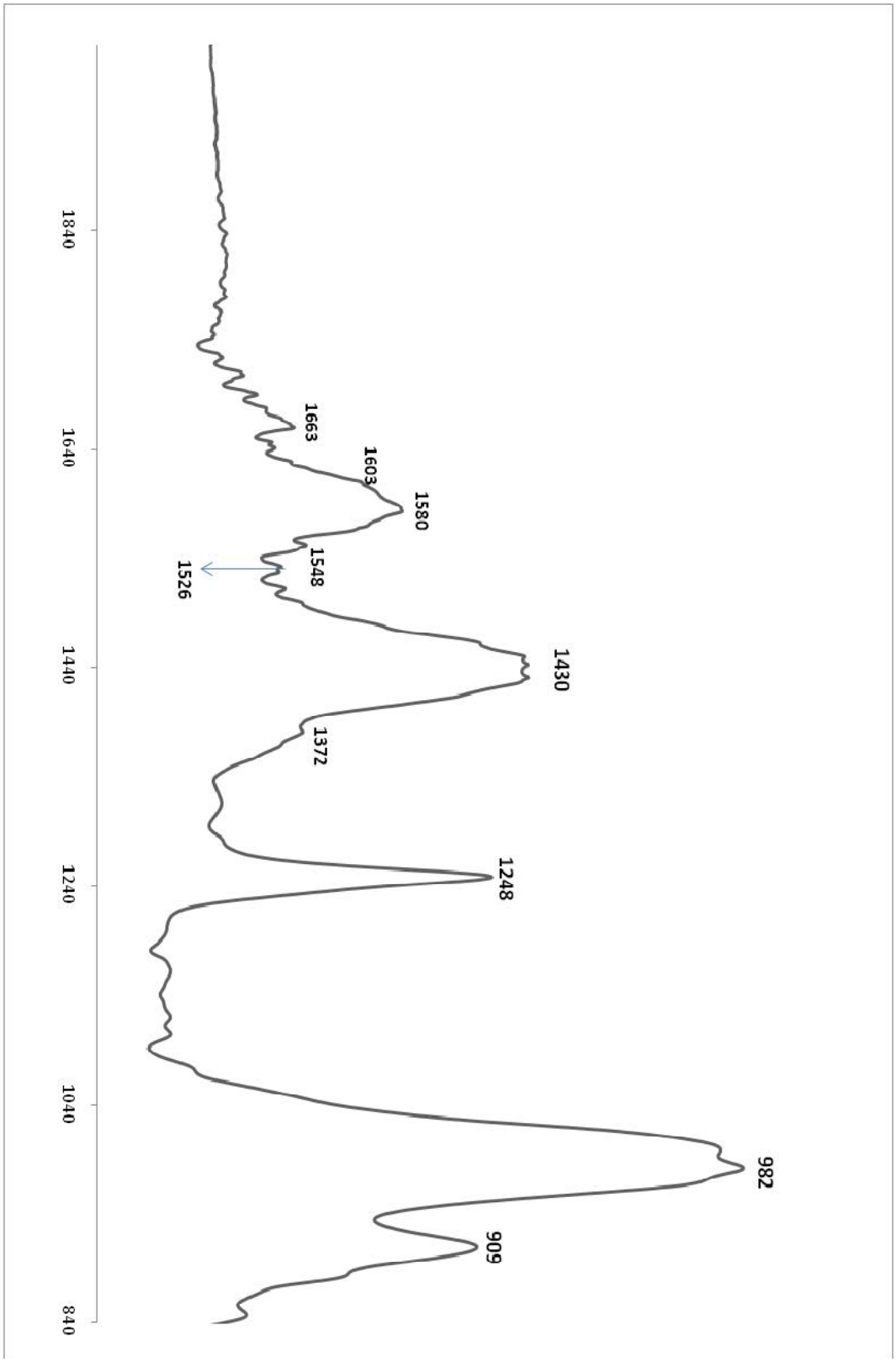

Figure 3-22. IR spectrum of $[Fe^{I}OEPone]^{-}$ in KBr matrix

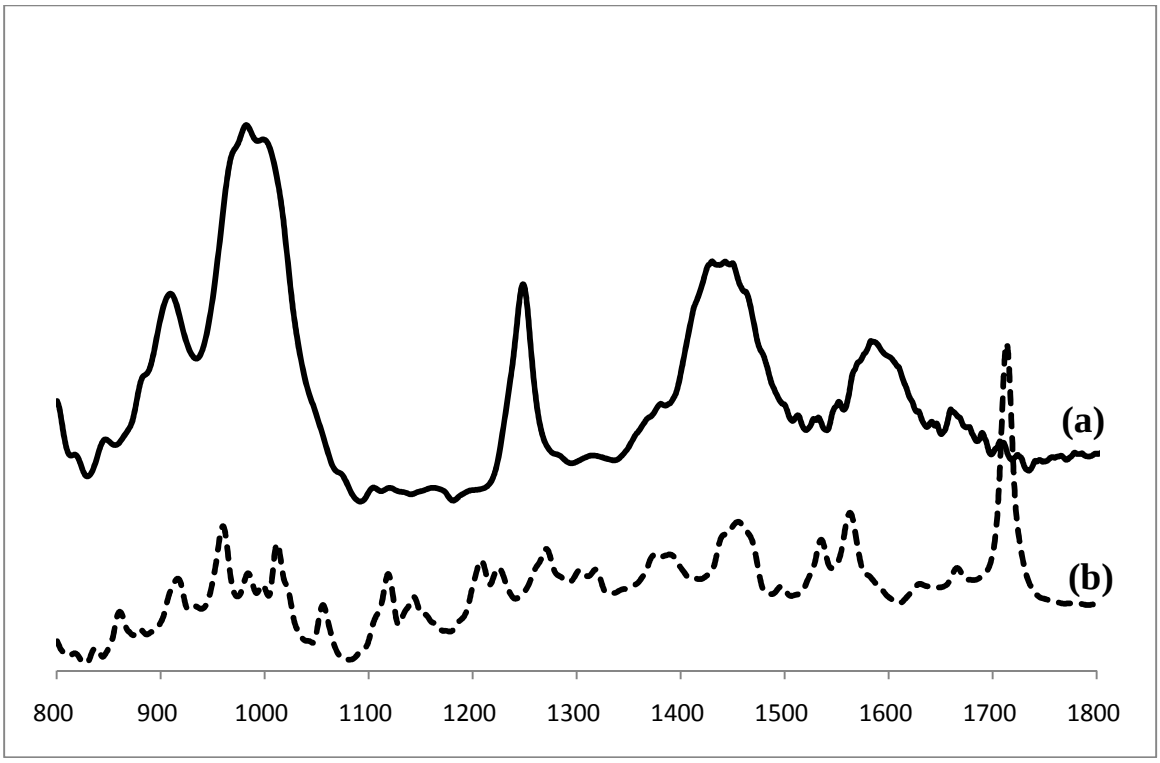

Figure 3-23. Infrared spectrum of (a) $[FeOEPone]^-$ (solid line) and (b) $Fe^{III}(OEPone)Cl$ (dash line) which have been obtaineded in KBr matrix.

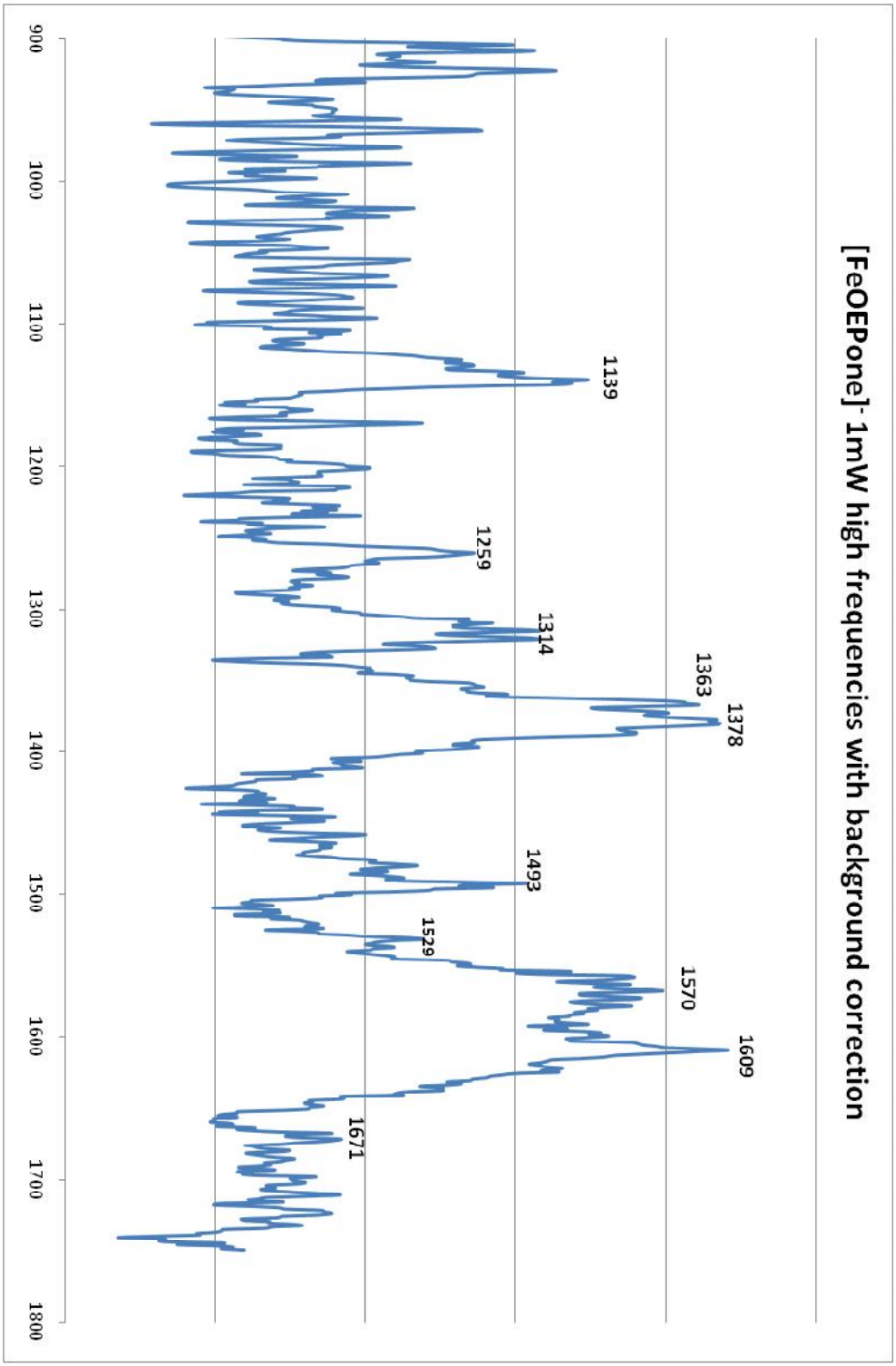

Figure 3-24. The low frequency resonance Raman spectrum of $[FeOEPone]^-$ with 406 nm excitation line at room temperature in KBr matrix with background correction. The power was 1.0 – 0.9 mW and the correction time is three hours.

3-7. CONCLUSIONS:

The ultimate goal of the work was to obtain the x-ray structure of $[Fe^{I}OEPone]^{-}$. The crystallization was carried out with the method by Reed[40]. The crude product of $[Fe^{I}OEPone]^{-}$ was dissolved in dibenzo-18-crown-6 in pyridine and THF solution to obtained the crystal $[NaDB\text{-}18\text{-}crown\text{-}6(THF)_2][Fe(OEPone)]$ for X-ray analysis. However, crystallization with dibenzo-18-crown-6 was unsuccessful, and the temporary loss of the department x-ray diffractometer prevented further attempts at crystallization. Future studies should incorporate the crown ether into the sodium anthracenide solution to minimize the synthetic steps and prevent oxidation of the iron(I) product.

The deuteration of porphinone complexes are quite important for the porphinone studies because: 1) the deuteration can reduce the complexity of the infrared spectrum by eliminating the vibration bands between 1400 cm^{-1} to 1500 cm^{-1}; 2) the deuteration at other positions would help with the assignment of the infrared bands.

The reduction of iron(III) tetraphenylporphyrin and octaethylporphyrin complexes were moderately finished with the method by Reed[13] and some impurities due to iron(II) were observed. The infrared spectra are examined to obtain the reduction's influence on the vibration modes between 1000 cm^{-1} to 1700 cm^{-1}. However, much better success was achieved for the iron porphinone, which was the goal of this work.

The Raman spectra of reduction product $[Fe^{I}OEPone]^{-}$ were obtained in KBr matrix.

The infrared and Raman spectrum for $[Fe^{I}OEPone]^{-}$ will allow us to compare the spectrum data to the DFT calculation results that have done by Ryan[38], which will help us better understand the structure and the electron properties of $[Fe^{I}OEPone]^{-}$.

REFERENCE:

1. http://en.wikipedia.org/wiki/Porphyrin

2. Woodward, R. B.; Skaric, V. ***J. Am. Chem. Soc.*** *1961, 83, 4676*

3. Bonnett, R.; Gale, I. A. D.; Stephenson, G. F. ***J. Chem. Soc*** *1967, 1168*

4. Grigg, R.; Sweeney, A.; Johnson, A. W. ***J. Chem. Soc. D*** *1970,1237*

5. Paine, J. B., 111; Dolphin, D. ***J. Am. Chem. Soc.*** *1971, 93, 4080*

6. Kenner, G. W.; Smith, K. M.; Sutton, M. **J. *Tetrahedron Lett.*** *1973, 1303*

7. Barkigia, K. M.; Fajer, J.; Spaulding, L.D.; Williams, G. ***J. Am. Chem. Soc*** *1981, 103, 76*

8. Janick, R.A. Ph.D. **Thesis**, Duke University, 1982

9. Reed, C.A., Mashiko, T., Bentley, S.P., Kastner, M.E., Scheidt, W.R., Spartalian, K., Lang, G., ***J .Am. Chem. Soc.***, *1979, 101, 2948*

10. Boersma, A.D., Goff, H.M. ***Inorg. Chem.*** *1982, 21, 581*

11. Scheidt, W.R., ***Acc. Chem. Res.,*** *1977, 10, 339*

12. Scheit, W.R., Reed, C. A. ***Chem. Rev.,*** *1981, 81, 543*

13. Reed, C. A. ***Adv. Chem. Ser.*** *1982, No. 201, 333-356*

14. Donohoe, R.J; Atamian, M.; Bocian, D. F. ***J. Am. Chem. Soc.*** *1987, 109, 5593-5559*

15. Spiro, T.G. In Iron Porphyrins, Lever, A. B. P., Gray, H. B., Eds.; ***Addison- Wesley: Reading, MA***, 1983; Vol. II, pp 89-159

16. Giraudeau, A.; Callot, H. J.; Jordan, J.; Ezhar, I.; Gross, M. ***J. Am.Chem. Soc.*** *1979, 101, 3857-3862*

17. Kadish, K. M.; Boisselier-Cocolios, B.; Simonet, B.; Chang, D.; Ledon, H.; Cocolios, P. ***Inorg. Chem.*** *1985, 24, 2148-2156*

18. Giraudeau, A.; Louati, A,: Gross, M.; Callot, H. J.: Hanson, L. K.; Rhodes, R. K.;

Kadish, K. M. ***Inorg. Chem.*** *1982, 21, 1581-1586*

19. Kitagawa, T.; Teraoka, J. ***The Biological Chemistry of Iron***; Dunford, H. B., Dolphin, D., Raymond, K. N., Sieker, L., Eds.; D. Reidel Dordrecht: Holland, 1982; p 375.

20. Solovyov, K. N.; Gladkov, L. L.; Starukhin, A. S.; Shkirman, S. F. ***Spectroscopy of Porphyrins: Vibrational Stale; Nauka: I Tekhnika*** *1985*

21. Spiro, T. G. Iron Porphyrins Lever, A. B. P., Gray, H. B., Eds.; ***Addison-Wesley: Reading,*** *1983; Vol. 2, p 91*

22. Spaulding, L.; Chang, C.; Yu, N.; Felton, H. ***J. Am. Chem. Soc.****1974, 96, 2517-2525*

23. Spiro, T. G.; Strekas, T. C. ***J. Am. Chem. Soc.*** *1974, 96, 338*

24. Kitagawa, T.; Iizuka, T.; Ikeda-Saito, M.; Kyogoku, Y. ***Chem. Lett.*** *1975, 849*

25. Kitagawa, T.; Kyogoku, Y.; Iizuka, T.; Ikeda-Saito, M. ***J. Am. Chem. Soc.*** *1976, 98, 5169*

26. Kitagawa, T.; Teraoka, ***J. Chem. Phys. Lett.*** *1979, 63, 443*

27. Spiro, T. G.; Stong, J. D.; Stein, P. ***J. Am. Chem. Soc.*** 1979, *101,* 2648

28. Teraoka, J.; Kitagawa, T. ***J. Phys. Chem.*** 1980, 84, 1928

29. Kashiwagi, H.; Obara, S. Int. ***J. Quani. Chem.*** *1981, 20, 843*

30. Abe, M.; Kitagawa, T.; Kyogoku, Y. ***J. Chem. Phys.*** *1978, 69, 4526*

31. Cohen, I. A.; Ostfeld, D.; Lichtenstein, B. ***J. Am. Chem. Soc.*** *1972, 94, 4522*

32. Chang, C.K.; Sotiriou, C.; ***J. Heterocyclic Chem.*** *1985, 22, 1739*

33. Hickman, D.L.; Shirazi, A.; Goff, H. M. ***Inorg. Chem.*** *1985, 24, 563-566*

34. Yamaguchi.K, Morishima,I. ***Inorg. Chem.*** *1992, 31, 3216*

35. Neal, T.; Kang, S.; Turowska-Tyrk, H.; Schulz, C; Scheidt, W. ***Inorg. Chem.*** *2000, 39, 872-880*

36. Scheidt, W. R.; Lee, Y. J. ***Struct. Bonding (Berlin)*** 1987, *64,* 1.

37. Liu,Y.M., PH.D. thesis, Marquette University, 1998

38. Wei, Z., Ryan, M.D. ***Inorg. Chem.*** *2010, 49, 6948–6954*

39. Teraoka, J.; Hashimoto, S.; Sugimoto, H.; Mori, M.; Kitagawa, T. ***J. Am. Chem. Soc.*** *1987, 109, 180–184*

40. Mashiko, T.; Reed, C. A.; Haller, K. J.; Scheidt, W. R. ***Inorg. Chem.****1984, 23, 3192–3196*

41. Scheer, H.; Inhoffen, H. H. In ***The Porphyrins****;* Dolphin, D., Ed.; Academic: New York, 1978; Vol. 2, pp 45-50

42. Stolzenberg, A. M.; Glazer, P. A,; Foxman, B. M. ***Inorg. Chem.*** *1986, 25, 983*

43. Chang, C. K.; Barkigia, K. M.; Hanson, L. K.; Fajer, J. ***J. Am. Chem. Soc.*** *1986,108, 1352*

44. Liu, Y.; Ryan, M.D. ***Inorganica Chimica Acta*** *1994, 225, 57-66*

45. Lexa, D.; Momenteau, M.; Mispelter, ***J. Biochim. Biophys. Acta*** *1974, 338, 151*

46. Kadish, K. M.; Larson, G.; Lexa, D.; Momenteau, M. ***J. Am. Chem. Soc.*** *1975, 97, 282*

47. Wei, Z., PHD thesis, Marquette University

48. Kincaid, J. R.; Urban, M. W.; Watanabe, T.; Nakamoto, K. ***J. Phys. Chem.*** *1983, 87, 3096–3101*

49. Li, X.-Y.; Czernuszewicz, R. S.; Kincaid, J. R.; Stein, P.; Spiro, T. G. ***J. Phys. Chem.*** *1990, 94, 47–61*

50. Ogoshi, H.; Masai, N.; Yoshida, Z.; Takemoto, J.; Nakamoto, K.Bull. ***Chem. Soc. Jpn.*** *1971, 44, 49–51*

51. Paulat, F.; Praneeth, V. K. K.; Nather, C.; Lehnert, N. ***Inorg. Chem.*** *2006, 45, 2835–2856*

52. Mylrajan, M.; Andersson, L. A.; Loehr, T. M.; Wu, W.; Chang, C. K. ***J. Am. Chem. Soc.*** *1991, 113, 5000–5005*

53. Cai, S., Belikova, E., Yatsunyk, L. A., Stolzenberg, A. M., Walker, F. A. ***Inorg. Chem.*** *2005, 44, 1882-1889*

54. Alder, A. D; Longo, F.R.; Finareli, J. D.; Goldmacher, J.; Assour, J.; Korsakoff, L. ***J. Org. Chem.*** *1967, 32, 467*

55. Inhoffen, H. H.; Nolte, W. ***Liebigs Ann. Chem.*** *1969, 725, 167.*

56. Dolphin, D. *"**The porphyrins**" Vol. 1, pp. 414, New York, 1978.*

57. Stolzenberg A. M.; Stauss, S. H.; Holm, R. H. ***J. Am. Chem. Soc.*** *1981, 103, 4763*

58. Stolzenberg, A.M.; Laliberte, M. A. ***J. Org. Chem.*** *1987, 52, 1022-1027*

59. Chang, C. K.; Sotiriou, C. ***J. Org. Chem.*** *1987, 52, 926*

60. Chang, C.K.; Sotiriou, C. ***J. Org. Chem.*** *1985, 50, 4989*

61. Wu, W.; Chang, C. K. ***J. Am. Chem. Soc.*** *1987, 109, 3149*

62. Chang C.K.; Sotitiou C.; Wu *W.* ***J. Chem. Soc.*** 1986, 1213 – 1215

63. Burke, J. M.; Kincaid, J. R; Peters, S.; Gagne, R.R.; Collman, J. P.; Spiro, T. G. ***J. Am. Chem. Soc.*** 1978, 100, 6083-6088